Materials Today Bio 12 (2021) 100158

Contents lists available at ScienceDirect

Materials Today Bio

journal homepage: www.journals.elsevier.com/materials-today-bio

The balanced microenvironment regulated by the degradants of appropriate PLGA scaffolds and chitosan conduit promotes peripheral nerve regeneration

Panjian Lu [a,1], Gang Wang [a,1], Tianmei Qian [a], Xiaodong Cai [a], Ping Zhang [a], Meiyuan Li [a], Yinying Shen [a], Chengbin Xue [a,b,**], Hongkui Wang [a,*]

[a] Key Laboratory of Neuroregeneration of Jiangsu and Ministry of Education, Co-innovation Center of Neuroregeneration, NMPA Key Laboratory for Research and Evaluation of Tissue Engineering Technology Products, Nantong University, Nantong, China
[b] Jiangsu Clinical Medicine Center of Tissue Engineering and Nerve Injury Repair, Research Center of Clinical Medicine, Affiliated Hospital of Nantong University, Nantong, China

ARTICLE INFO

Keywords:
PLGA
Schwann cells
Regeneration microenvironment
Inflammation

ABSTRACT

Tissue-engineered nerve grafts (TENGs) are the most promising way for repairing long-distance peripheral nerve defects. Chitosan and poly (lactic-co-glycolic acid) (PLGA) scaffolds are considered as the promising materials in the pharmaceutical and biomedical fields especially in the field of tissue engineering. To further clarify the effects of a chitosan conduit inserted with various quantity of poly (lactic-co-glycolic acid) (PLGA) scaffolds, and their degrades on the peripheral nerve regeneration, the chitosan nerve conduit inserted with different amounts of PLGA scaffolds were used to repair rat sciatic nerve defects. The peripheral nerve regeneration at the different time points was dynamically and comprehensively evaluated. Moreover, the influence of different amounts of PLGA scaffolds on the regeneration microenvironment including inflammatory response and cell state were also revealed. The modest abundance of PLGA is more instrumental to the success of nerve regeneration, which is demonstrated in terms of the structure of the regenerated nerve, reinnervation of the target muscle, nerve impulse conduction, and overall function. The PLGA scaffolds aid the migration and maturation of Schwann cells. Furthermore, the PLGA and chitosan degradation products in a correct ratio neutralize, reducing the inflammatory response and enhancing the regeneration microenvironment. The balanced microenvironment regulated by the degradants of appropriate PLGA scaffolds and chitosan conduit promotes peripheral nerve regeneration. The findings represent a further step towards programming TENGs construction, applying polyester materials in regenerative medicine, and understanding the neural regeneration microenvironment.

1. Introduction

Tissue-engineered nerve grafts (TENGs) are currently the most promising way to repair long-distance peripheral nerve defects [1–3]. Tissue engineering contains three essential factors, including biological materials, supporting cells, and growth factors. Based on quite a few researches, either biomaterial-based nerve neural conduit or the TENGs with seed cells, cytokines, or extracellular matrix, TENGs achieved

Abbreviations: TENG, tissue-engineered nerve graft; PLGA, poly (lactic-co-glycolic acid); PGA, poly (glycolic acid); PLA, poly (lactic acid); SCs, Schwann cells; DMEM, Dulbecco's modified eagle medium; SD, Sprague-Dawley; FBS, fetal bovine serum; DAPI, 4' 6-diamidino-2-phenylindole; CCK8, Cell Counting Kit-8; OD, optical density; NC, negative control; TUNEL, terminal deoxynucleotidyl transferase-mediated dUTP-biotin nick end labeling; NS, normal saline; SFI, sciatic nerve function index; CMAPs, compound muscle action potentials; HE, hematoxylin-eosin; α-BGT, α-bungarotoxin; SD, standard deviation; ANOVA, one-way analysis of variance.

* Corresponding author.
** Corresponding author. Key Laboratory of Neuroregeneration of Jiangsu and Ministry of Education, Co-innovation Center of Neuroregeneration, NMPA Key Laboratory for Research and Evaluation of Tissue Engineering Technology Products, Nantong University, Nantong, China.
E-mail addresses: 1257225540@qq.com (P. Lu), 1446118564@qq.com (G. Wang), qiantm86@ntu.edu.cn (T. Qian), 1332452108@qq.com (X. Cai), 3309556098@qq.com (P. Zhang), limeiyuan1986@ntu.edu.cn (M. Li), 1047928046@qq.com (Y. Shen), xuechengbin@ntu.edu.cn (C. Xue), wanghongkui@ntu.edu.cn (H. Wang).
[1] These authors have contributed equally to this work.

https://doi.org/10.1016/j.mtbio.2021.100158
Received 17 September 2021; Received in revised form 10 November 2021; Accepted 13 November 2021
Available online 16 November 2021

continuous progress [4–7]. As the core element of tissue engineering, the discovery and creation of new biomaterials are the fastest growing and the most innovative field [8–11]. Biomaterials for tissue engineering are more demanding than general applications in biocompatibility and biodegradability. Biological materials are generally divided into natural materials and synthetic materials, whose research and selection are crucial for the better construction of TENGs. Natural materials have superior compatibility, while synthetic materials have superior plasticity.

Chitosan is a natural polymer biomaterial with rich sources and excellent biocompatibility that is the only essential amino polysaccharide and has been proven to regulate and suppress inflammation [12,13]. Given the advantages of chitosan, we developed a TENG using chitosan as the primary material, which was the patented product (No. ZL 0110820.9, china). The chitosan-based TENG could make full use of the body's regenerative ability to drive reprogramming of endogenous cells and aids peripheral nerve function recovery in the form of in situ tissue regeneration [14–16]. The TENG is composed of two parts: the nerve conduit and the scaffolds inserted in a lumen. The fiber scaffolds added into the nerve conduit aim to further imitate the axial architectural structure inside natural nerves to guide the Schwann cell migration and axon regeneration [17,18]. Peripheral nerve regeneration microenvironment refers to the local inflammatory and immune state jointly presented by main cells including Schwann cells, macrophages, vascular endothelial cells, fibroblasts, biomaterials, and physical and chemical factors in the regeneration chamber, which is crucial to nerve regeneration [19–21]. Unlike the neural conduit, which needs to maintain sufficient strength for a relatively long period to maintain the local regenerative microenvironment, the fiber scaffolds inserted are demanded to be degraded soon after the guidance effect is completed, so as to leave space for further nerve regeneration and tissue remodeling. The poly (lactic-co-glycolic acid) (PLGA), a widely researched and applied synthetic polymer material, was selected as the guide scaffolds inside the TENG. The PLGA scaffolds neutralize the rapid degradation of poly (glycolic acid) (PGA) and the slow degradation of poly (lactic acid) (PLA).

Our team has continued to perform researches in-depth on the chitosan/PLGA based TENG for decades, involving the effectiveness assessment of TENGs repairing the peripheral nerve defect, the safety evaluation of TENGs causing the inflammation and immune reactions, and the improvement exploration of TENGs combining supporting cells and growth factors [22–25]. Moreover, a few studies on chitosan shaped into the nerve conduit have been conducted, such as its good biocompatibility with nerve cells and vascularization after implanted *in vivo*, its effects of reducing the wrong projections of regenerative axons compared with the end-to-end suture, and its mechanisms of the degradation product facilitating peripheral nerve regeneration [26–30]. However, the PLGA scaffolds in the lumen of TENG, directly guiding the growth of Schwann cells (SCs) and nerve axons, have few relevant studies about its functions except for the preliminary observation of cell-directing effects of the scaffolds [31]. Compared with the chitosan nerve conduit, the aspects of the PLGA scaffolds about the degradation products and degradation rate, the impact on the regenerative microenvironment, and its interaction with nerve cells directly affect peripheral nerve regeneration.

PLGA is a polyester material copolymerized with PGA and PLA, widely studied and used in regenerative medicine [32–35]. With the deepening of researches, it is gradually recognized that the acidic degradation product of PLGA may limit its applications in the construction of tissue-engineered tissues and organs. However, there is literature on the effects of PLGA or similar materials on the local regeneration microenvironment *in vitro* and *vivo*, the illustration of which is ambiguous and sometimes contradictory [36–39]. Especially as an essential component of the TENGs, whether the acid degradation products are absolutely harmful to the nerve cells in the regeneration microenvironment or beneficial to the final results of peripheral nerve regeneration have not been precisely and thoroughly explored. It is critical but has no essential experimental supports that if it is necessary to add guiding scaffolds inside the neural conduit and if the degradation of scaffolds in the regenerative microenvironment significantly affects the biological behaviors of local cells. The explorations of questions will have a tremendous instructing sense for improving the design of the delicate internal structure of TENGs, the selection and application of the more suitable scaffold materials, and the further enhancement of the ability of clinical peripheral nerve injury repairs.

Our work aimed to observe and evaluate the influences of the different amounts of PLGA fiber scaffolds within the nerve conduit on the regenerative microenvironment. The TENGs containing 0 (conduit), 1 (conduit+1), 2 (conduit+2) and 3 (conduit+3) PLGA scaffolds woven from monofilaments were constructed to repair rat sciatic nerve defects. We jointly investigate the effects of cellular guidance and the degradation of PLGA scaffolds on the local regenerative microenvironment composed of different cells *in vitro* and *in vivo*. Our work will provide a solid theoretical foundation and guidance for a deeper understanding of the interaction between biomaterials and tissues in peripheral nerve regeneration microenvironment, a more rational design of the detailed structure of TENGs, and better repair of peripheral nerve defects in clinical practices.

2. Methods

2.1. PLGA extracts preparation

PLGA scaffolds were immersed and extracted in Dulbecco's modified eagle medium (DMEM) (Invitrogen, Carlsbad, CA, USA) at 37 °C with a proportion of 10.5 μl/cm that was equivalent to the scale of 3 PLGA scaffolds inserted in conduit *in vivo*. The pH value of the PLGA extraction liquid was detected by an electronic pH Meter (S–3C, REX, Shanghai, China). Hereafter, the influences of PLGA extraction liquid instead of DMEM media on the primary SCs *in vitro* were further evaluated.

2.2. Schwann cell culture

As previously described, primary SCs were isolated from the sciatic nerve of neonatal Sprague-Dawley (SD) rats [40]. Briefly, the sciatic nerve was dissected and treated with collagenase and trypsin. Collected cells were cultured in DMEM supplemented with 10% fetal bovine serum (FBS) (Invitrogen), 1% penicillin and streptomycin (Invitrogen), 2 μM forskolin (Sigma, St. Louis, MO, USA), and 10 ng/ml heregulin β1 (Sigma) till confluence. Cells were then treated with anti-Thy1.1 antibody (Sigma) and rabbit complement (Invitrogen) to remove fibroblasts. Purified SCs were grown in a culture medium containing DMEM, 10% FBS, and 1% penicillin and streptomycin (Invitrogen) in a humidified 5% CO_2 incubator at 37 °C. Primary SCs were passaged for no more than two passages before use. The purity of SCs was identified by immunocytochemical staining using the primary antibody rabbit anti-S100 (1:200 dilution, Abcam), and the second antibody goat anti-rabbit IgG-Cy3 (1:100 dilution, Abcam), and nucleus were labeled with 4',6-diamidino-2-phenylindole (DAPI) (SouthernBiotech).

2.3. Cell viability assay

The SCs viability was detected using Cell Counting Kit-8 (CCK8) (Dojindo, Kumamoto, Japan). In short, cells were seeded in a 96-well plate added culture medium or extraction liquid for 24 h. Then the CCK8 reagent (10μl/well) was added to each well followed an incubation for 2 h. The cell viability was indicated with the optical density (OD) value at 450 nm by a microplate reader (BioTek, USA). The experiment was repeated three times. The data of PLGA was normalized to that of negative control (NC).

2.4. Cell proliferation assay

The proliferation of SCs *in vitro* was examined using EdU proliferation assay as previously described [41]. Briefly, SCs were seeded on poly-L-lysine-coated 96-well plates at a density of 2×10^5 cells/ml. 50 μM EdU was added to the culture medium or extraction liquid, and SCs were cultured for an additional 12 h before fixation. Cell proliferation rate was calculated as the ratio of EdU positive cells to the number of total cells by a Cell-Light EdU DNA Cell Proliferation Kit (Ribobio, Guangzhou, Guangdong, China). Images were obtained under a fluorescence microscope (DMR, Leica Microsystems, Bensheim, Germany). The experiment was repeated three times. The three non-overlapping fields in each well were used for statistics.

2.5. Cell migration assay

The migration ability of SCs was tested using the Transwell migration assay. In brief, SCs with 3×10^5 cells/ml were resuspended in DMEM or extraction liquid and added to the top chamber of a Transwell with 8 μm pores (Costar, Cambridge, MA, USA). Then the 500 μl medium was added to the bottom chamber pre-coated with 10 μg/ml fibronectin. After 24 h, the upper surface of the top chamber was cleaned while the bottom surface was stained with 0.1% crystal violet. SCs adhering to the bottom surface were observed and photographed under an inverted microscope (Leica). The areas of migratory SCs were calculated using ImageJ software (https://imagej.nih.gov/ij/index.html). The data of PLGA was normalized to that of NC (fold change). The experiment was repeated three times. The three non-overlapping fields in each well were used for statistics.

2.6. Cell apoptosis assay

The SCs apoptosis *in vitro* and *in vivo* was detected using a terminal deoxynucleotidyl transferase-mediated dUTP-biotin nick end labeling (TUNEL) BrightGreen Apoptosis Kit (Vazyme, Nanjing, Jiangsu, China). In short, slides of cells cultured with media or extraction liquid for 24 h and tissues were marked through incubation with BrightGreen Labeling Mix and Recombination TdT Enzyme at 37 °C for 1 h, following a permeation with 20 μg/ml Proteinase K at room temperature for 10 min. Then, the nuclei were stained by DAPI (SouthernBiotech). Images of cells and tissues were observed and obtained under the fluorescence microscope (Axio Imager M2, Carl Zeiss Microscopy GmbH, Jena, Germany). The experiment was repeated three times. The three non-overlapping fields in each well were used for statistics.

2.7. TENGs preparation

TENGs were constructed, including chitosan conduits with 1 mm wall thickness and 2 mm inner diameter, and the different number of PLGA scaffolds. Briefly, the chitin/chitosan (Nantong Xincheng Biochemical, Nantong, China) mixtures were injected into stainless-steel casting molds, which were sealed and placed at −12 °C for 2–4 h and then lyophilized under a 35–45 mTorr vacuum for 20 h after rinsing [42]. The PLGA (PGA: PLA = 9:1) sutures were woven from 140 to 160 monofilaments, which was about 10 μm in diameter (Nantong Holycon, Nantong, China). The PLGA fibers, used as the guiding scaffolds, were inserted into the lumen of chitosan nerve conduit before surgery. The chitosan conduits alone (conduit) and conduits inserted with 1 (conduit+1), 2 (conduit+2) or 3 (conduit+3) PLGA scaffolds were pruned and stored in normal saline (NS) for bridging sciatic nerve defects.

2.8. Sciatic nerve defect model construction

The animals were divided into conduit, conduit+1, conduit+2, conduit+3 and autograft groups randomly (n=8) for evaluation at 4 w, 8 w and 12 w three time points. Adult female SD rats about 200 g were acquired from the Experimental Animal Center of Nantong University (License No. SYXK (Su) 2017–0046). The animals were housed in a temperature-controlled environment and allowed food and water ad libitum. The Administration Committee approved all experimental protocols of Experimental Animals, Jiangsu Province, China, following the guidelines of the Institutional Animal Care and Use Committee, Nantong University, China (Inspection No: 20180301–009). All rats were deeply anesthetized by an intraperitoneal injection of compound anesthetic (chloral hydrate 4.25 g, magnesium sulfate 2.12 g, sodium pentobarbital 886 mg, ethanol 14.25 ml, and propylene glycol 33.8 ml in 100 ml). The skin and muscle were incised to expose the sciatic nerve at the left mid-thigh. An 8-mm segment of the sciatic nerve was resected to form a 10 mm gap following a slight retraction of the nerve stumps [42]. The sciatic nerve defects were bridged by TENGs or autologous nerves. Finally, the muscle layers and skins were closed with sutures.

2.9. Gait analysis

The integrated function recovery was assessed via Catwalk XT 9.0 (Noldus, Wageningen, Netherlands) gait analysis system. Animals were allowed to pass through a glass walkway, underneath which a video camera captured each run. The sciatic nerve function index (SFI) was calculated and analyzed to reflect functional recovery, including motor and sensory functions. The values of animals subjected to toes ulceration or curling were excluded. SFI=109.5 (ETS-NTS)/NTS-38.3 (EPL-NPL)/NPL+13.3 (EIT-NIT)/NIT-8.8 (TS is toe spread. PL is print length. IT is intermediate toe spread. E and N indicate the experimental and normal contralateral hind paws, respectively.).

2.10. Electrophysiology analysis

Under deep anesthesia with compound anesthetic, the surgical site at the left mid-thigh level was reopened, and the sciatic nerve was re-exposed. Electrical stimuli were applied to the sciatic nerve trunk at the distal and proximal ends of the graft sequentially. Compound muscle action potentials (CMAPs) were recorded on the gastrocnemius belly. The assessments of normal sciatic nerve CMAPs were conducted at the uninjured contralateral side.

2.11. Tissue sample collection and processing

Animals were anesthetized and perfused via the ascending aorta with NS and 4% paraformaldehyde. The regenerated nerves in the mid-graft segment were harvested. The bilateral gastrocnemius and tibialis anterior muscles were removed and measured to calculate the wet weight ratio. The collected nerves and gastrocnemius muscles were then post-fixed for 6–8 h at 4 °C, frozen, and cut into 12-μm-thick slices, respectively.

2.12. Inflammation score

The inflammation grade of the local regeneration microenvironment was semiquantitatively scored and evaluated by hematoxylin-eosin (HE) staining of the cross-section in the middle segment of the bridge (ISO 10993–6: 2007) [43–45]. Three random fields with high magnification (× 400) in the lumen of conduit per animal were used for inflammation score. Images were photographed under upright microscopy (Zeiss).

2.13. Masson trichrome and motor endplate staining

The cross-sections of the gastrocnemius (12 μm) were subjected to Masson trichrome staining to calculate the average cross-sectional area of muscle fibers. The muscle cells in 5 random fields with high magnification (× 400) per animal were selected for cross-sectional area statistics. The longitudinal sections of the gastrocnemius (25 μm) were subjected toα-bungarotoxin (α-BGT) (1:200 dilution, Sigma) staining for 12 h at

room temperature to calculate the average area of motor endplates, which were combined with immunohistochemical staining of mouse anti-PGP 9.5 (1:200 dilution, Gene Tex). The motor endplates in 9 random fields with high magnification (× 400) per animal were calculated for area statistical analysis. Images were photographed under upright microscopy (Zeiss). The areas of muscle fibers and motor endplates were counted by ImageJ software (https://imagej.nih.gov/ij/index.html).

2.14. Immunohistochemical staining

The immunohistochemical staining of the cross-section of regenerated nerve in the middle segment of the bridge was performed to analyze the nerve regeneration, cell proliferation, blood vessel, and macrophage. The sections were blocked with 5% goat serum for 1 h at 37 °C, incubated with primary antibodies overnight at 4 °C, and then incubated with secondary antibodies for 1 h at room temperature. Primary antibodies included mouse anti-NF200 antibody (1:200 dilution, Sigma), rabbit anti-S100 antibody (1:200 dilution, Abcam), mouse anti-S100 antibody (1:1000 dilution, Sigma), rabbit anti-Ki67 antibody (1:200 dilution, Sigma), goat anti-CD34 antibody (1:50 dilution, R&D), rabbit anti-Iba1 antibody (1:25 dilution, Wako), mouse anti-CD68 antibody (1:100 dilution, Abcam), rabbit anti-CD206 antibody (1:100 dilution, Abcam) and mouse anti-PGP 9.5 (1:200 dilution, Gene Tex). Secondary antibodies included goat anti-mouse IgG-Alex-488 (green) (1: 500 dilution, Abcam), goat anti-rabbit IgG-Cy3 (red) (1:100 dilution, Abcam), donkey anti-goat IgG-Alex-488 (green) (1:500 dilution, Abcam), and sheep anti-rabbit IgG-Cy3 (red) (1:1000 dilution, Abcam). Nuclei were marked using Hoechst 33342 (blue) (1:5000 dilution, Life Technologies). Images were acquired under fluorescence microscopy (Zeiss). The entire space of conduit lumen was collected for statistics on the area of regenerated nerves and the number of blood vessels and macrophages. In addition, the three random fields with high magnification (× 400) in the lumen of conduit per animal were picked for the cell proliferation, cell apoptosis, and macrophage sort analysis. The quantities of immunofluorescence were conducted by calculations of the positive signal areas using ImageJ software (https://imagej.nih.gov/ij/index.html).

2.15. Scanning electron microscope

Samples of biomaterials were fixed in 4% glutaraldehyde and post-fixed with1% OsO_4, dehydrated in a graded series of ethanol, which were replaced by *tert*-butyl alcohol. Afterward, samples processed were dried in a freeze drier (Hitachi, ES-2030, Japan) and then mounted for scanning electron microscope observation after platinum coating.

2.16. Transmission electron microscope

The animals were anesthetized and then perfused with a fixative containing 1% paraformaldehyde and 1.25% glutaraldehyde. The regenerating nerves in the middle segments and gastrocnemius muscles were collected, postfixed in 4% glutaraldehyde, and embedded in Epon 812 epoxy resin (Sigma). Ultrathin sections were obtained and stained with lead citrate and uranyl acetate. The morphology of nerves and muscles were observed under a transmission electron microscope (JEOL Ltd., Tokyo, Japan). The three random fields with low magnification (× 1.2k) per animal were chosen for myelinated nerve fiber statistics involving the g-ratio (nerve axon diameter/nerve fiber diameter) and thickness of myelin. The five random fields with high magnification (× 20.0k) per animal were selected for the count of myelin sheath layers.

2.17. Statistical analysis

The numerical results were presented as means ± standard deviation (SD). Unpaired *t*-test was used for mean comparison between two groups. One-way analysis of variance (ANOVA) was used for mean comparisons among multiple groups (Tukey's multiple comparisons test). Statistical analysis was conducted by using Graph-Pad Prism 6.0 software (Graph-Pad Software Inc., La Jolla, CA, USA). A p-value< 0.05 was considered statistically significant.

3. Results

3.1. Effects of abundant PLGA degradation products on SCs in vitro

First of all, the pH of PLGA scaffolds extraction liquid was measured. The media without PLGA scaffolds, as the negative control, had almost no changes both in the appearance color and pH value as expected (Fig. 1A). However, the color of the extraction liquid obviously changed with a macroscopic thinning of PLGA scaffolds at 4 w (Fig. 1A). Correspondingly, the pH value indicated that the degradation of a great amount of PLGA scaffolds makes the medium gradually acidified at 2 w and 4 w (Fig. 1B). Especially the acidity of extract liquid increased significantly, reaching 3.41 at 4 w (Fig. 1B). The effects of the acid extraction liquid at 4 w on the behaviors of primary cultured SCs were subsequently tested. The SCs were identified following purification (Fig. S1). Not surprisingly, the robust acidic environment caused by the degradation of excessive PLGA scaffolds firstly exerted a significant adverse effect on the viability of SCs (Fig. 1C). Then, by detecting of the basic biological behaviors *in vitro*, the acid extraction of PLGA greatly inhibited the proliferation and migration of SCs and significantly induced apoptosis of SCs (Fig. 1D-F).

3.2. Axon and Schwann cell regrowth

The sciatic nerve defects were bridged by TENGs containing 0, 1, 2 and 3 PLGA scaffolds that were inserted into lumens of chitosan conduits: conduit, conduit+1, conduit+2 and conduit+3 respectively (Fig. 2). The tissue structure, mainly the axons and SCs, was panoramic and dynamically displayed via immunochemical staining of the middle segment of the regenerated nerve. The room and protection provided by the chitosan nerve conduit for nerve regeneration *in vivo* were suitable and stable. The tube wall of nerve conduit had sufficient strength to maintain complete regeneration space at 4 w and 8 w. Then, the lumen was slightly compressed due to the gradual degradation of biomaterials at 12 w, which was compatible with the densification and remodeling of tissue architecture of regenerated nerve (Fig. 3A). However, the area of axons and SCs demonstrated significant differences between different groups. The areas of axons and SCs of conduit+1 were significantly larger than those of other TENGs at all three-time points (Fig. 3A-D). In addition, there was always no significant difference in the area of regenerated axons between the conduit+1 and autograft, while the area of SCs of autograft, as the positive control, was more significant (Fig. 3A-D). The nerve regeneration of the conduit was slightly worse than those of conduit+2 and conduit+3 groups without statistical difference at 4 w (Fig. 3B). The differences in nerve regeneration among different groups could be more intuitively displayed through a dynamic form. It could also be noted that the area of regrown axons and SCs from 8 w to 12 w was reduced, which should undergo remodeling and maturation (Fig. 3E). Meanwhile, in the axial section of conduit+1, it was demonstrated that SCs migrated along the PLGA scaffolds and further guided axon regeneration, and the regenerated nerve had grown over the entire nerve defect and entered the distal nerve trunk (Fig. S2). Moreover, the area percentage of PLGA/lumen of the TENG with different amounts of PLGA scaffolds was calculated (4.13%, 7.63%, and 12.75%), which suggested that the addition of scaffolds could have minor adverse effects on the space of conduit lumen for nerve regeneration (Fig. S3) [46]. Therefore, more PLGA fibers were not considered. The excessive space occupation of guiding scaffolds would inhibit peripheral nerve regeneration.

3.3. Regenerative nerve ultrastructure

The structure and quality of myelinated scaffolds of regenerated

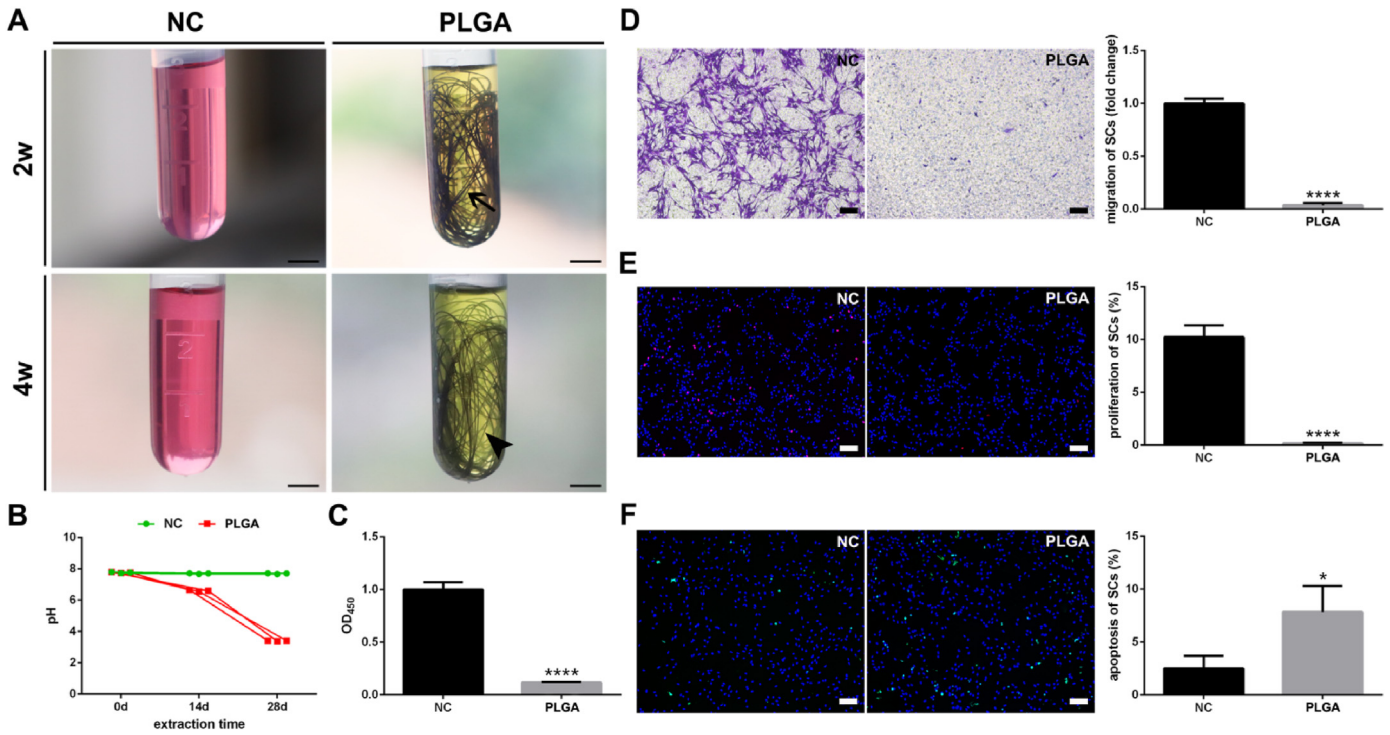

Fig. 1. Degradation of numerous PLGA scaffolds and its influence on SCs *in vitro*. (A) The appearance changes of PLGA submerged in DMEM. The massed PLGA scaffolds immersed in a limited volume of medium imitated the 3 PLGA scaffolds inserted into the chitosan nerve conduit. Arrow indicated PLGA scaffolds at 2 w. Arrowhead indicated significantly thinner PLGA scaffolds at 4 w. Scale bar, 500 μm. (B) The pH values of PLGA extraction liquid. The acidity of the media continued to increase with the degradation of materials. (C–F) The degradation products of exorbitant PLGA at 4 w greatly inhibited cell viability using CCK8 detection (C), migration using Transwell assay (purple) (D), and proliferation using EdU assay (red) (E), and induced apoptosis using TUNEL assay (green) (F). Nuclei were blue in (E) and (F). *, PLGA group vs. NC group. *, $p<0.05$; ****, $p<0.0001$. Scale bar, 100 μm.

nerve were analyzed more precisely from the ultrastructural level through transmission electron microscopy. The differences in the mean of the axon diameter and myelin thickness of the regenerated nerve scaffolds among the groups were demonstrated, which was critical to the quality of nerve functional recovery. However, the advantages as guessed in remyelination of conduit+1 were not demonstrated at 4 w after surgery. The g-ratio, the thickness of myelin, and the number of myelin layers were comparable among three biomaterial groups, which were inferior to the autograft group (Fig. 4A and B). However, as the repair time passed to 8 w, the potential for myelin regeneration of conduit+1 was beginning to be displayed. The indicator mentioned above of conduit+1 was significantly better than those of conduit, conduit+2, and conduit+3 groups, and gradually approached autograft (Fig. 4A and C).

Nevertheless, the g-ratio of the conduit was slightly better than the other two TENGs with more PLGA scaffolds (Fig. 4C). At 12 w after surgery, the thickness of myelin and the number of myelin layers of the conduit+1 still demonstrated much better recovery than conduit, conduit+2, and conduit+3 groups (Fig. 4A and D). Meanwhile, the g-ratio showed an identical situation, although the difference was not statistically significant (Fig. 4D). However, it was not the same that the difference between the autograft and conduit+1 in parameters was statistically significant (Fig. 4D). The evolution of remyelination of different repair biomaterials in the process of nerve regeneration and the differences between them was further unequivocally painted in the dynamic diagrams (Fig. 4E).

3.4. Target muscle reinnervation

As nerves innervated the target organs, the muscles would undergo denervation atrophy after nerve injuries. It was distinctly revealed that the muscle atrophy and subsequent recovery of conduit+1 were better than conduit+2 and conduit+3 groups and closer to the autograft group. At 4 w post-surgery, the wet weight ratios of anterior tibialis of conduit, conduit+2 and conduit+3 groups were significantly less than those of conduit+1 and autograft; while the wet weight ratios of gastrocnemius of conduit+2, and conduit+3 groups except for conduit were also significantly lower than those of conduit+1 and autograft (Fig. 5F). Then the wet weight ratios of two target muscles of conduit+1 and autograft were better than those of the other three groups at 8 w and 12 w after surgery (Fig. 5G and H). However, the muscle weight advantage of conduit+1 compared to the conduit+2 and conduit+3 groups was more prominently displayed on gastrocnemius atrophy at 8 w and 12 w (Fig. 5G and H). The comprehensive dynamic charts demonstrated that the performance of better-reinnervated target muscles of conduit+1 and autograft, as the denervated muscles first atrophied and then recovered (Fig. 5I). In addition, compared with the gastrocnemius muscle, the anterior tibialis muscle continued to atrophy more significantly after denervation (Fig. 5I).

Hereafter the cross-sectional areas of gastrocnemius muscle fibers were calculated and analyzed (Fig. 5A-E). In the images of Masson trichrome, it was presented that the areas of muscle fibers of conduit+1 and autograft were significantly larger than those of other groups at all time points (Fig. 5A). Meanwhile, the different degrees of collagen fiber hyperplasia between muscle cells were displayed. At 8 w and 12 w after surgery, the collagen fibers between muscle fibers of conduit+1 and autograft were less than those of other groups (Fig. 5A). The statistical results confirmed that the muscle fiber cross-sectional areas of the conduit, conduit+2, and conduit+3 groups were significantly smaller than those of conduit+1 and autograft (Fig. 5B-D). The difference in the area of myocytes among groups was the smallest at 4 w. There was no statistically significant difference in muscle cell area between conduit and conduit+1 (Fig. 5B). Afterward, the more vital recovery ability of target muscles of conduit+1 and autograft in the later stage of nerve regeneration was evidently illustrated through the dynamic analysis

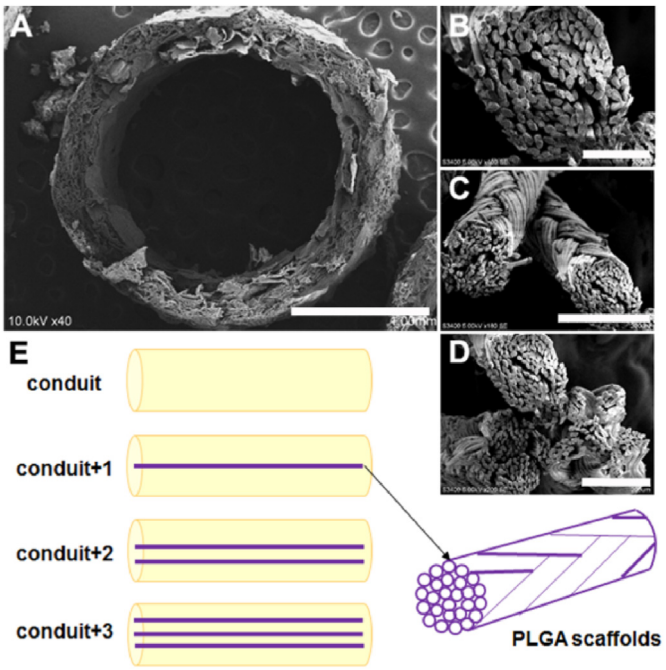

Fig. 2. Constructions of the TENGs with different number of PLGA scaffolds. (A) Scanning electron eicroscope picture of cross section of chitosan nerve conduit. The wall of nerve conduit displayed a multi-layered porous structure. Scale bar, 1 mm. (B–D) Scanning electron eicroscope pictures of cross sections of 1, 2 and 3 PLGA scaffolds. The PLGA scaffolds were woven from multiple monofilaments. Scale bar, 100 μm, 300 μm, and 200 μm respectively. (E) Schematic diagrams of the TENGs assembled with nerve conduits and different amounts of PLGA scaffolds.

(Fig. 5E). Moreover, the areas of the motor endplates of the gastrocnemius were further counted to assess the reinnervation of the target muscles. From all three time points, the areas of neuromuscular junctions of conduit+1 and autograft were significantly larger than those of conduit, conduit+2, and conduit+3 groups (Fig. 6A-D), and the disparities between them were pretty obvious (Fig. 6E).

Meanwhile, of note, a few muscle samples of conduit+1 and autograft had already seen the nerve endings reinnervating the target muscles, but none of the other three groups at 8 w after surgery (Fig. S4). Moreover, the nerve endings branching into the motor endplates of conduit+2 and conduit+3 groups could not be stained and detected in parts of muscle slices until 12 w post-surgery. Finally, the ultrastructure of the denervated gastrocnemius of different groups were also observed and compared. The loss and recovery of normal ultrastructure of muscle fibers in two-time points of conduit+1 and autograft were significantly better than those in other groups. At 4 w after surgery, the disorder of original neat structure and the apparent myofibril disintegration was shown, and the increased amount of mitochondria with degenerative vacuole changes were displayed of conduit, conduit+2, and conduit+3 groups (Fig. S5). At 12 w after surgery, the normal ultrastructure of muscle fibers had recovered to a certain extent, and a few swollen mitochondria were still visible of conduit, conduit+2, and conduit+3 groups (Fig. S5).

3.5. Nerve impulse conduction

The measurements of regenerative nerve electrophysiology also uncovered the superiority of conduit+1 in repairing nerve defects. At all three time points, the electrophysiological function recovery of the other three groups, including conduit, conduit+2, and conduit+3 groups, showed significant deficiencies from conduit+1 (Fig. 7A-D). Furthermore, the differences in the ability to conduct nerve impulses mentioned above were more evident at 12 w (Fig. 7D). Meanwhile, there was no statistical difference of the CMAPs by electrophysiological evaluations between conduit+1 and autograft, although the two groups had a slight disparity at 12 w (Fig. 7D). From the dynamic point of view, the primary recovery stage of CMAPs was in the late period of nerve regeneration accompanied by the myelination of axons from 8 w to 12 w post-surgery (Fig. 7E). This more critical period of recovery of nerve conduction function showed the advantages of CMAPs of conduit+1 and autograft over the others. Correspondingly, the measurement and analysis of SFI also demonstrated that the overall functional recovery of conduit+1 was better than other TENG groups and similar to that of the autologous nerve repair (Fig. S6).

3.6. Macrophage and blood vessel of regenerative microenvironment

The infiltration of macrophages and the formation of new blood vessels are the most common parameters for studying the foreign reaction of biomaterials implanted *in vivo*. So all macrophages and blood vessels involved in the cavity of the TENG at 4 w after surgery were observed and analyzed. Above all, macrophages and vasculatures were roughly evenly distributed and not accumulated excessively near the PLGA scaffolds or some other sites in all groups (Fig. 8A). The further statistical analysis illustrated the differences in the number of macrophages and blood vessels among the TENGs containing different quantities of PLGA scaffolds. The area of neovascularization of conduit+3 was slightly larger than that of conduit+2 with no statistical significance (Fig. 8B). However, the blood vessels of conduit+2 and conduit+3 groups were significantly more redundant than those of conduit, conduit+1, and autograft (Fig. 8B). Additionally, due to the implantation of biomaterials, the number of macrophages of autograft was significantly less than those of all TENGs (Fig. 8B). Furthermore, similar to the blood vessels, the macrophages of conduit+2 and conduit+3 groups were significantly more than those of conduit and conduit+1 (Fig. 8B). However, it was displayed that the infiltration of macrophages of conduit was more than that of conduit+1, but with no significant difference too (Fig. 8B). In addition, in tissue regeneration, macrophages show different polarization types, namely pro-inflammatory M1 subset and anti-inflammatory M2 subset [47].

Does the existence and degradation of PLGA scaffolds affect macrophages' polarization state in the local microenvironment? The statistical results showed that macrophages' types were consistent with the intensity of local inflammation of different groups with different PLGA scaffolds. In terms of the number and ratio of M1 macrophages, the significantly lower values were revealed of conduit+1 and autograft, while the values of conduit, especially conduit+2 and conduit+3 groups, were significantly higher (Fig. 8C). On the contrary, the number of M2 macrophages of conduit+1 was the highest of all groups (Fig. 8C). However, the highest ratio of M2 macrophages was that of autograft because of its lowest amount of total macrophages (Fig. 8C). Meanwhile, the ratio of M2 macrophages of conduit+1 was still significantly higher than conduit+2 and conduit+3 groups but was equivalent to that of conduit without a statistical difference (Fig. 8C).

3.7. Inflammation score of regenerative microenvironment

In addition to assessing the macrophages and blood vessels in the local regenerative microenvironment, more cell type and tissue structure changes were taken into account to score the local inflammatory response of different groups at 4 w after surgery. The cells, including polymorphonuclear cells, lymphocytes, plasma cells, and giant cells, and the tissue reactions including necrosis, fibrosis, and fat infiltration were involved and counted (Fig. 9A). The inflammation score of autograft was the lowest indicating the slightest local reaction, which was statistically different from other groups (Fig. 9B). Then the inflammation scores of conduit+2 and conduit+3 groups were significantly higher than that of conduit+1 (Fig. 9B), which was demonstrated mainly in terms of the

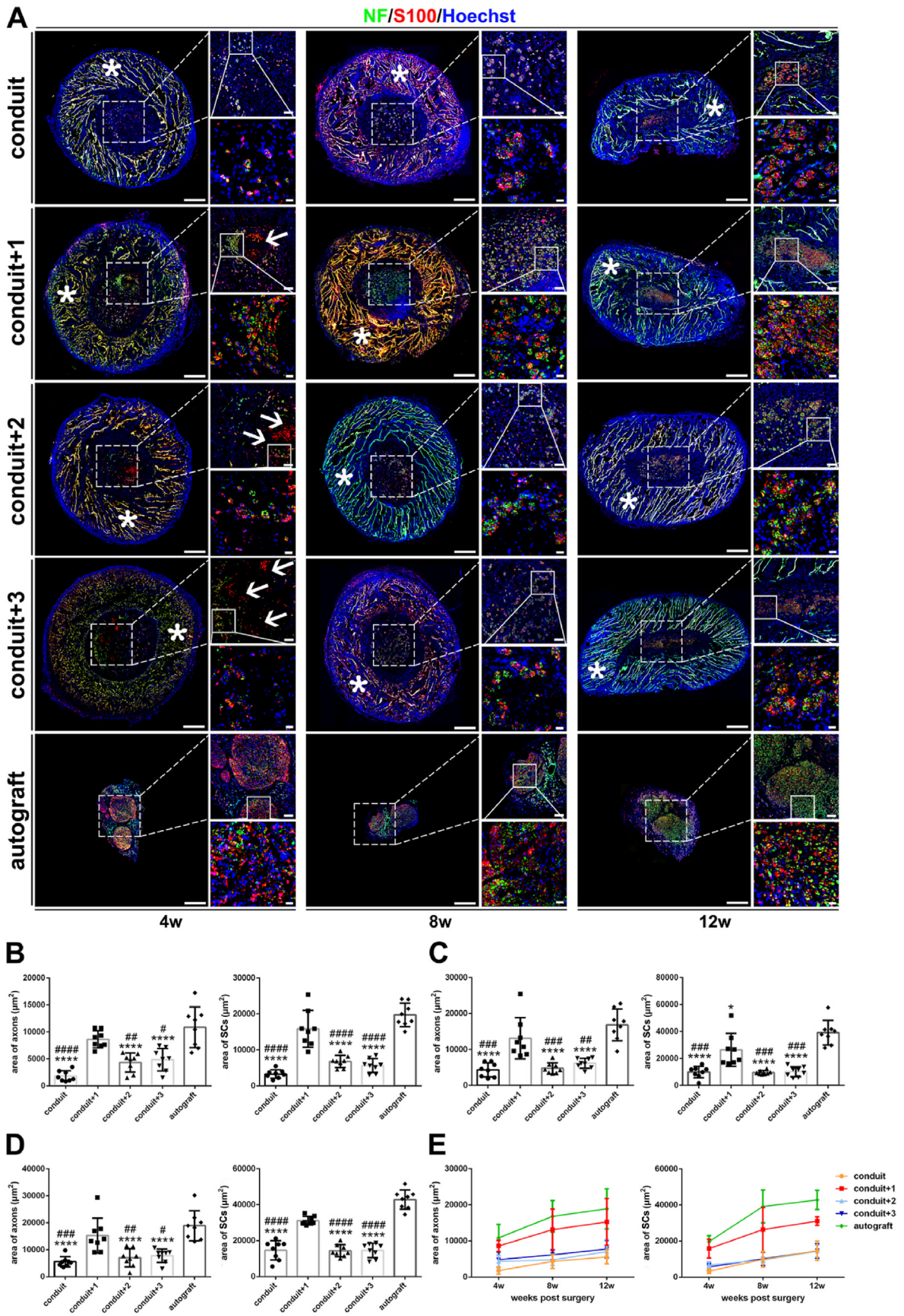

(caption on next page)

Fig. 3. The evaluation of axons and SCs regrowth displayed by immunohistochemistry. At the three observation time points, the regrowth of axons and SCs of conduit+1 were significantly better than those of the other three TENGs and were closer to the autograft. However, the difference in the area of SCs between conduit+1 and autograft was statistically significant at 12 w. (A) Panoramic images and low and high magnification fields stained by anti-NF (green) indicating axons, and anti-S100 (red) indicating both myelinated and non-myelinated SCs. Nuclei were stained using Hoechst (blue). The asterisks indicated the chitosan nerve conduits with the autofluorescence of biomaterials. The arrows indicated the different amounts of PLGA scaffolds inserted into the conduits. Scale bar, 500 μm, 100 μm, and 20 μm respectively. (B–D) Histograms of axons and SCs areas in the lumens of TENGs at 4 w, 8 w, and 12 w after surgery. *, each group vs. autograft group. #, each group vs. conduit+1 group. *, $p<0.05$; ****, $p<0.0001$. #, $p<0.05$; ##, $p<0.01$; ###, $p<0.001$; ####, $p<0.0001$. (E) Dynamic line charts of regrown axons and SCs at continuous time.

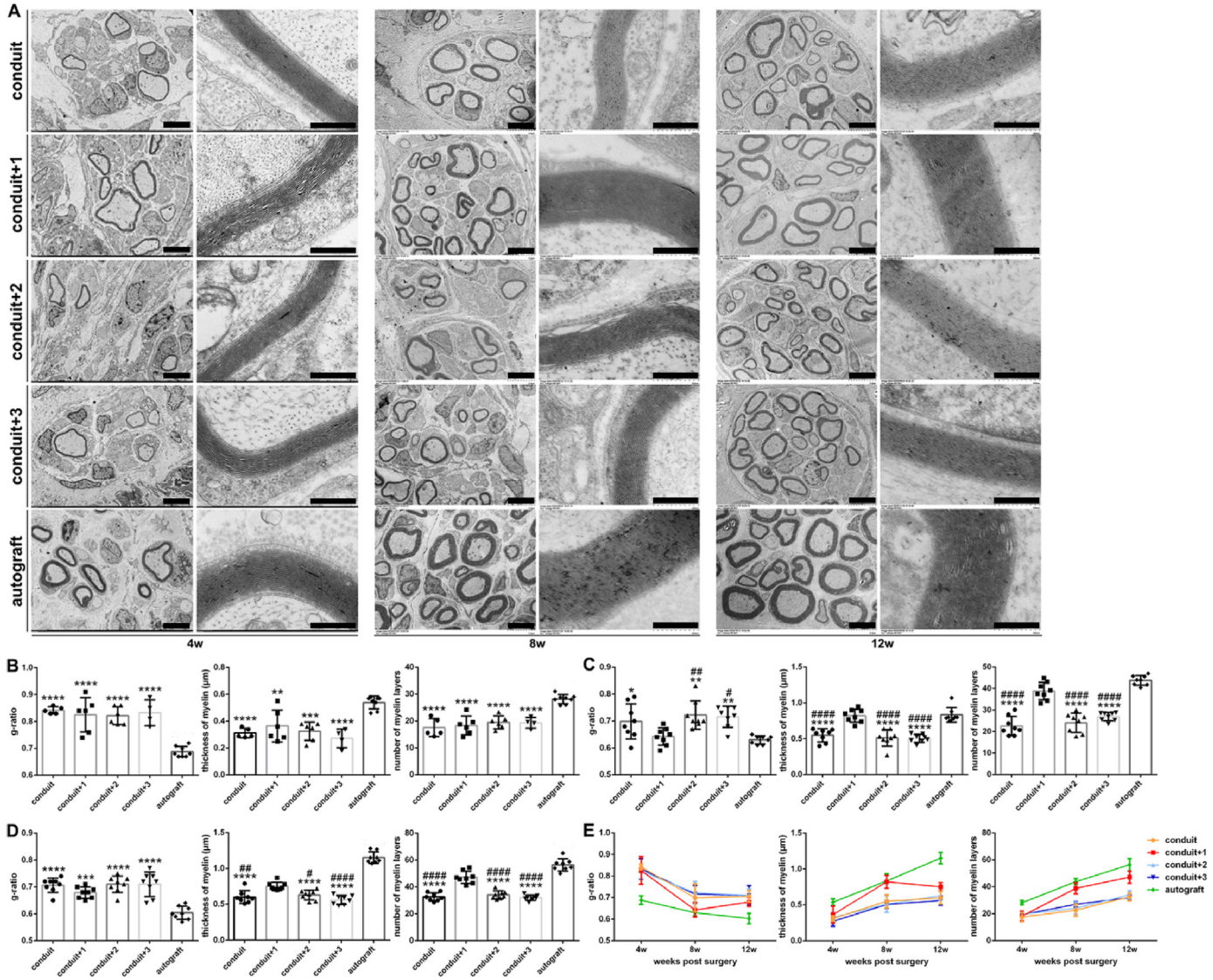

Fig. 4. The Ultrastructure of regenerated nerves under a transmission electron microscope. The significant advantage in the average thickness of myelin of conduit+1, compared with other TENGs, was reflected at 8 w and 12 w after surgery. At 4 w, the myelin regeneration of conduit+1 was similar to other TENGs, which were both different from the autograft. However, at 12 w after surgery, a certain difference of regenerated myelin between the conduit+1 and autograft existed. (A) The electron microscopic images of regenerated nerves, including magnified myelin sheaths. Scale bar, 5 μm and 500 nm. (B–D) Histograms of g-ratio, the thickness of myelin, and the number of myelin layers at 4 w, 8 w, and 12 w after surgery. *, each group vs. autograft group. #, each group vs. conduit+1 group. *, $p<0.05$; **, $p<0.01$; ***, $p<0.001$; ****, $p<0.0001$. #, $p<0.05$; ##, $p<0.01$; ####, $p<0.0001$. (E) Dynamic line charts of the parameters.

number of inflammatory cells (Fig. S7). Moreover, the conduit+3 group owned the highest inflammation score of all groups and significantly differed from the conduit group (Fig. 9B). Meantime, although the difference was not statistically significant, the implantation reaction of conduit+1 was slightly less than that of conduit, which unlocked that the alkaline degradation products of chitosan could also cause a slight inflammatory reaction in suit (Fig. 9B). Likewise, compared with the autograft, the inflammation grade was slight (3–8.9) of conduit+1 group (5.88), moderate (9-15) of conduit (10) group and conduit+2 group (13.88), and sever (>15) of conduit+3 group (17.75) respectively (Fig. 9C). We also calculated the thickness of the fibrous capsule formed on the surface of the nerve conduit implanted *in vivo*, and there were no significant differences among the groups (Fig. S8). The results unraveled that the inflammatory response of TENGs was predominantly limited to the inside of the nerve conduit, indicating that the difference should be caused by the degradation of different amounts of PLGA scaffolds.

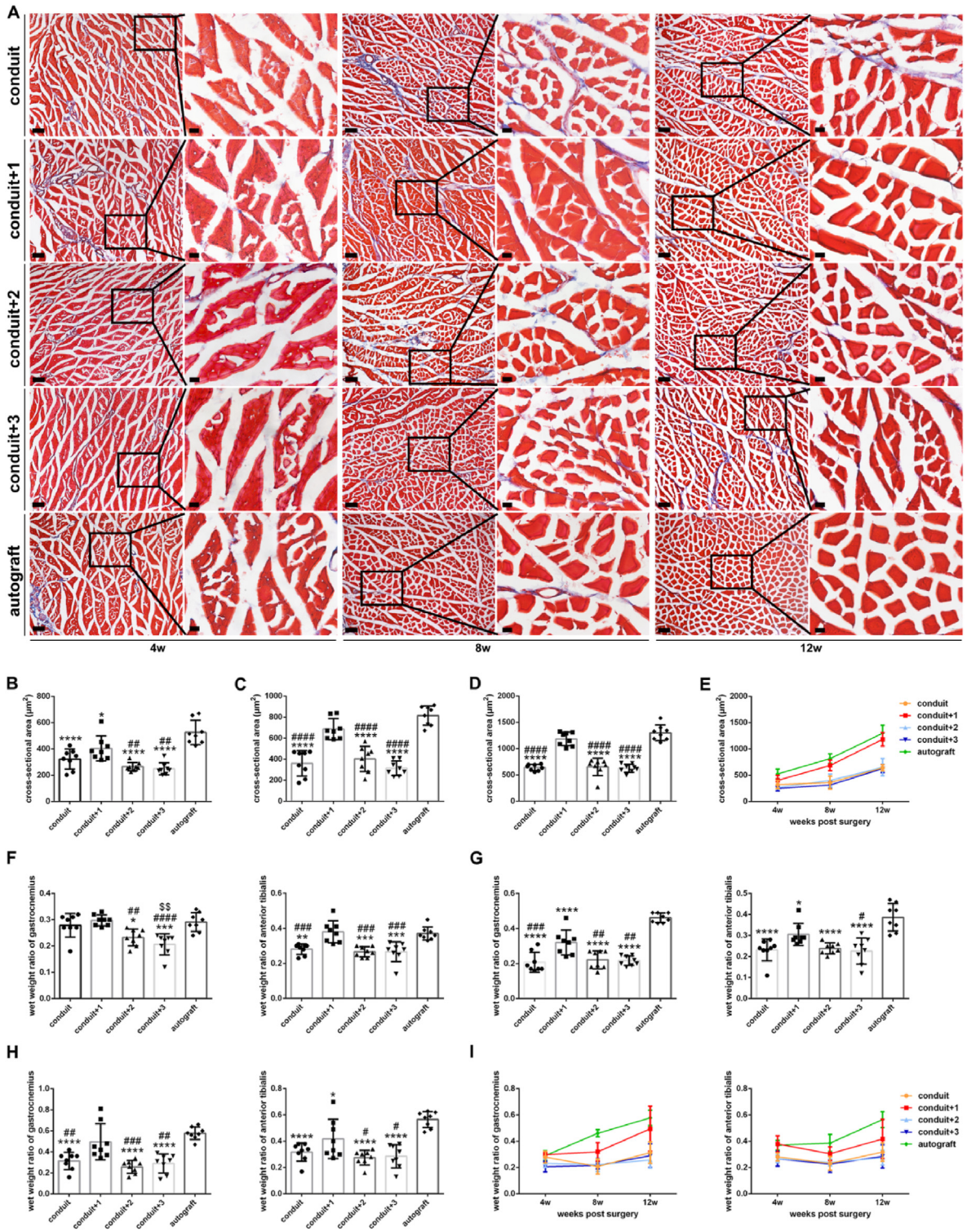

Fig. 5. The denervation atrophy and reinnervation recovery of target muscles. From the weight of target muscles, including gastrocnemius and anterior tibialis, to the average cross-sectional area of gastrocnemius cells, the statistical results demonstrated that the muscle atrophy and recovery of the conduit+1 were better than the other TENG groups and were closer to the autograft; proving the advantages and disadvantages of nerve regeneration and reinnervation among the groups. Moreover, the differences mentioned above of different bridging materials appeared more obvious as the repair time passed. (A) Masson trichrome staining of the gastrocnemius. Muscle fibers emerged red. Collagen fibers appeared blue. Scale bar, 100 μm, and 20 μm. (B–D) Histograms of the average cross-sectional areas of muscle fibers at 4 w, 8 w, and 12 w after surgery. (E) Dynamic line charts of the areas of muscle fibers. (F–H) Histograms of the wet weight ratios of the gastrocnemius and anterior tibialis at 4 w, 8 w, and 12 w after surgery. (I) Dynamic line charts of the wet weight ratios of target muscles. *, each group vs. autograft group. #, each group vs. conduit+1 group. *, $p<0.05$; **, $p<0.01$; ***, $p<0.001$; ****, $p<0.0001$. #, $p<0.05$; ##, $p<0.01$; ###, $p<0.001$; ####, $p<0.0001$.

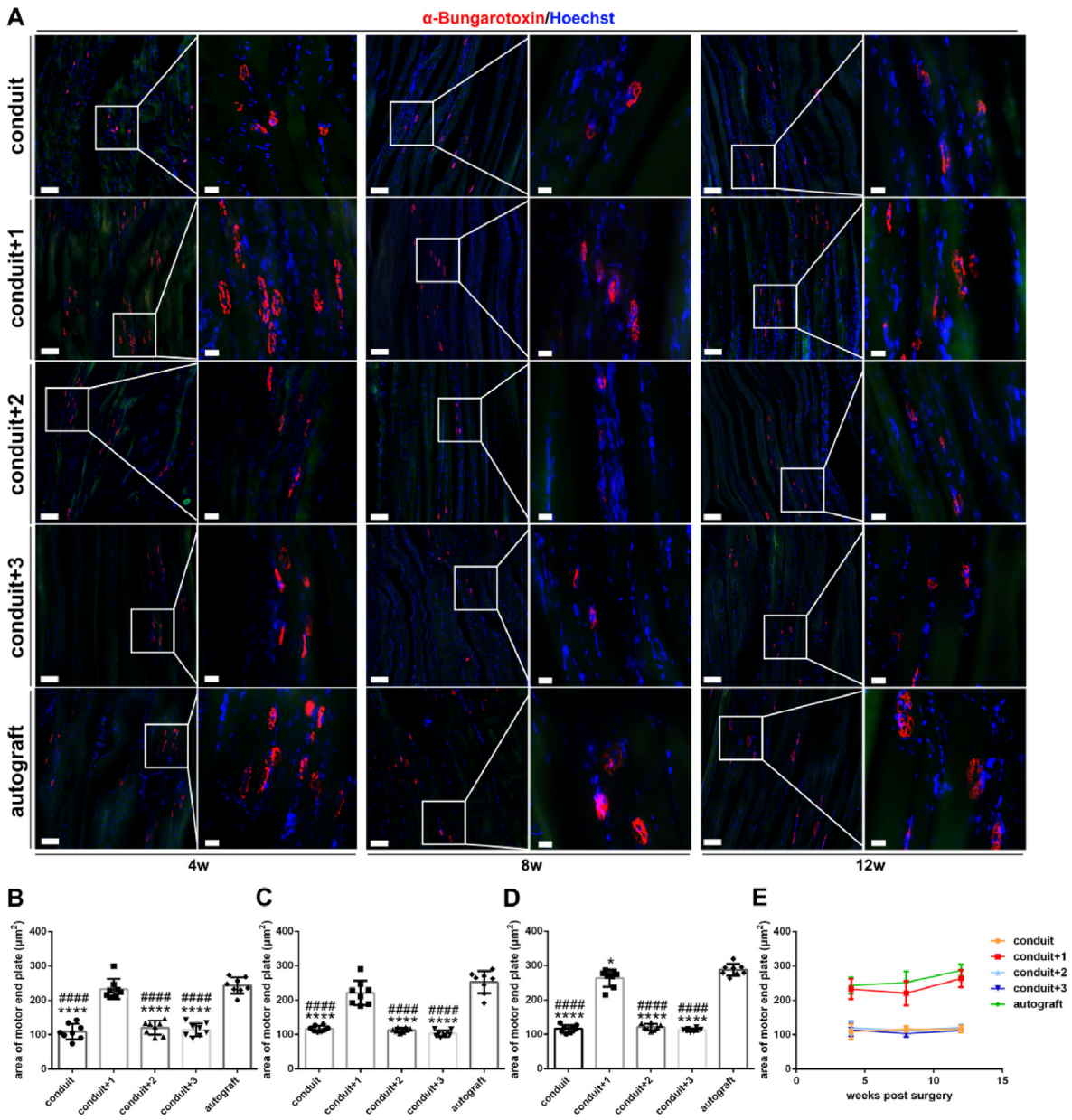

Fig. 6. The motor endplate staining of the gastrocnemius. At all three time points, the conduit and autograft groups' average areas of motor endplates were much bigger than those of the conduit, conduit+2, and conduit+3 groups. (A) The motor endplates were presented usingα-bungarotoxin staining (red). Nuclei were stained using Hoechst (blue). The longitudinal muscle fibers were displayed with light green autofluorescence instead of antibody labeling to better present the tissue structure. Scale bar, 100 μm, and 20 μm. (B–D) Histograms of the average areas of motor endplates. *, each group vs. autograft group. #, each group vs. conduit+1 group. *, $p<0.05$; ****, $p<0.0001$. ####, $p<0.0001$. (E) Dynamic line charts of the average areas of motor endplates.

3.8. Cell proliferation and apoptosis of regenerative microenvironment

Since the addition of PLGA scaffolds could cause significant changes in the inflammatory response of the regeneration microenvironment, what impacts the presence and quantity of PLGA scaffolds had on the behavior and status of local cells *in vivo*? The proliferation and apoptosis of cells, especially SCs, in the regenerated nerve at 4 w after surgery were detected and analyzed (Fig. 10A). From the point of view of the proliferation and apoptosis number and ratio, the autograft was the lowest due to its minimal regenerative microenvironment changes, significant differences from other TENG groups (Fig. 10B and C). In addition, the microenvironment of conduit, conduit+2, and conduit+3 groups inhibited cell proliferation to varying degrees compared to conduit+1 group (Fig. 10B). The proliferating cells were further divided into SCs and non-SCs. Proliferating non-SCs showed similar changes to all proliferating cells calculated, that is, the local microenvironment of the conduit, conduit+2, and conduit+3 groups inhibited cell proliferation (Fig. 10B). However, the proliferating SCs between the conduit+1, conduit+2, and conduit+3 groups had no statistical difference (Fig. 10B).

Interestingly, no matter the number and proportion of proliferating SCs, the conduit was significantly higher than the other three material groups (Fig. 10B). Of note, the statistics of SC proliferation unveiled another vital factor that may affect SC proliferation, namely the influence of scaffold guidance on SC proliferation and differentiation. Similarly, the local microenvironment of different TENGs also had a direct impact on cell apoptosis. From the total cell population to SCs or non-SCs, the conduit+2 and conduit+3 groups both induced more cell apoptosis than that of conduit+1 (Fig. 10C). Meanwhile, the cell apoptosis of conduit, especially the ratio of SC apoptosis, was slightly higher than that of

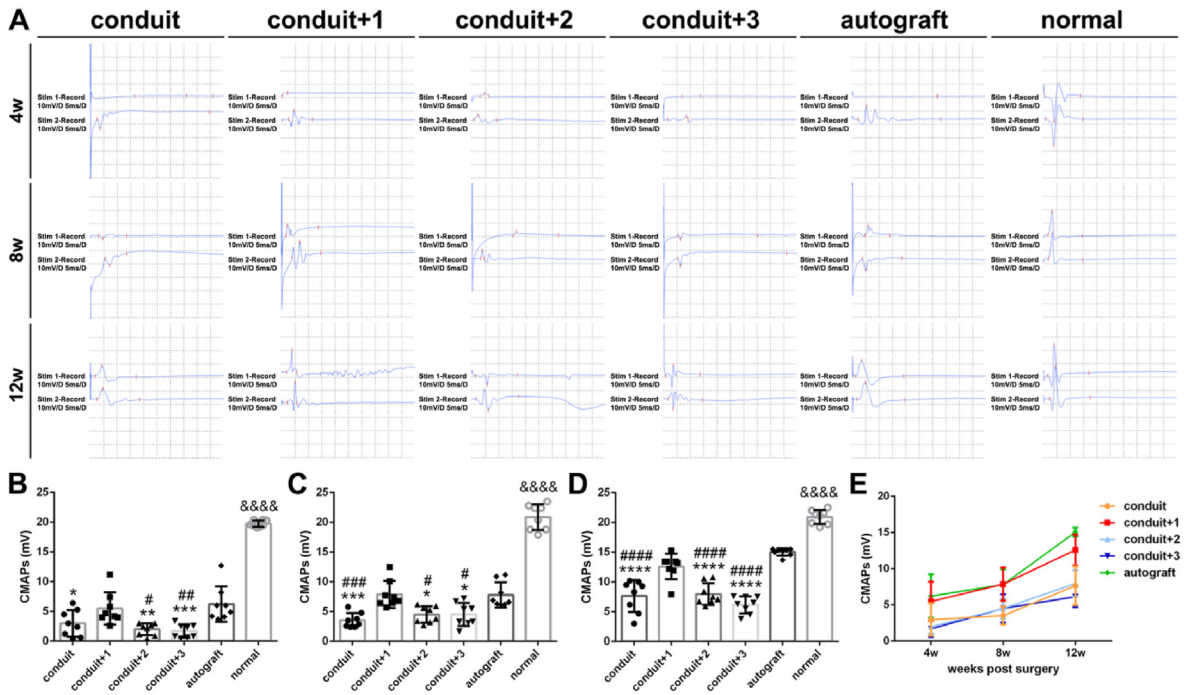

Fig. 7. The compound muscle action potentials of the gastrocnemius. The amplitudes of compound muscle action potentials of conduit+1 were significantly higher than those of the other three TENG groups. (A) The electrophysiological evaluation waveforms of the gastrocnemius. The distal (Stim 1) compound muscle action potentials and proximal (Stim 2) trunk of sciatic nerves were both recorded. (B–D) Histograms of the amplitudes of compound muscle action potentials at 4 w, 8 w, and 12 w after surgery. *, each group vs. autograft group. #, each group vs. conduit+1 group. &, each group vs. normal group. *, $p<0.05$; **, $p<0.01$; ***, $p<0.001$; ****, $p<0.0001$. #, $p<0.05$; ##, $p<0.01$; ###, $p<0.001$; ####, $p<0.0001$. &&&&, $p<0.0001$. (E) Dynamic line charts of the amplitudes of compound muscle action potentials.

conduit+1 without significant difference (Fig. 10C).

4. Discussion

PLGA, a synthetic polymer of classic polyester biomaterials, was widely studied and applied for the tissue regeneration and restoration. It was reported that PLGA, or PGA and PLA alone, was beneficial to the tissue regeneration including peripheral nerves [48–51]. With the deepening of researches involving observations in clinical trials, the possible adverse effects of acid degradation products of such biomaterials on regeneration were gradually recognized. However, the impact of this type of biomaterial on tissue repair is devoid of comprehensive and thorough observations and evaluations, which hinders further improvements and applications. The chitosan nerve conduit and PLGA scaffolds are jointly assembled to a TENG in the present work. The pointed study was designed and conducted to unravel the role and influence of PLGA scaffolds in TENGs during peripheral nerve regeneration. We focused on the impact of its degradation products on the regenerative microenvironment involving cells of the nervous system *in vivo*, which answered the critical questions about the necessity and amount of PLGA scaffolds added to the chitosan conduit.

Although it is known that the degradation products of PLGA are acidic, there is no intuitive understanding of its acidity. Unexpectedly, the acidification degree of the surrounding local space reached a quite high level after a large amount of degradation of PLGA scaffolds *in vitro*. The degradation products were more acid than the results of existing literature, which may be due to the different composition and quantity of the materials [36]. Not surprisingly, the strongly acidic extract liquid containing degradation products of the PLGA scaffolds significantly inhibited the vitality and biological behaviors of the primary cultured SCs. It requires to be further distinguished that the suppression of acid degradation products on cell biological behaviors was just caused via the cell viability reduction or other direct reasons. The TENGs containing the different number of PLGA scaffolds was used to bridge the sciatic nerve defects in rats. The three consecutive time points were selected for the assessment of nerve regeneration, so that a more comprehensive understanding of the dynamic process of peripheral nerve injury repair was painted. A substantial absorption of PLGA scaffolds was in about 30 d. So, the detection of the inflammation degree and cell status in the regeneration microenvironment was performed at 4 w after surgery. In addition, the PLGA scaffolds were completely absorbed in 60–90 d, which was confirmed by the experimental results *in vivo*.

In order to evaluate the influence of the number of PLGA scaffolds on nerve regeneration, the chitosan nerve conduit alone and the conduit containing 1, 2, or 3 PLGA scaffolds were constructed. It was demonstrated that the PLGA scaffolds act as a bridge to guide the SCs migration and axon regeneration [31]. Especially in the early stage, more regenerated nerves could be clearly seen around the PLGA scaffolds, explaining why the nerve regeneration of chitosan conduit only was poor. The assessment of nerve regeneration parameters delineated that conduit was even slightly worse than conduit+2 and conduit+3. On the contrary, more PLGA scaffolds including the conduit+2 and conduit+3 also resulted in the undesirable nerve regeneration. Since it took a considerable time for the envelopment and maturation of the myelin, the differences in the regeneration of TENGs with different number of PLGA scaffolds were further elucidated in detail by the ultrastructure observation. The advantage of remyelination of conduit+1 was unambiguously revealed with the extension of repair time. It was reflected that the number of myelinated nerve fibers of the autograft and conduit+1 was more than those of the other three groups, especially in the early stage. The difference in remyelination between groups was also reflected in the electrophysiological recovery. The CMAPs of conduit +1 equivalent to those of the autograft were significantly better than CMAPs of other groups at all-time points. Then the morphological and functional recoveries of the target muscles were analyzed from multiple levels. The results clearly described a typical change of the target muscle from

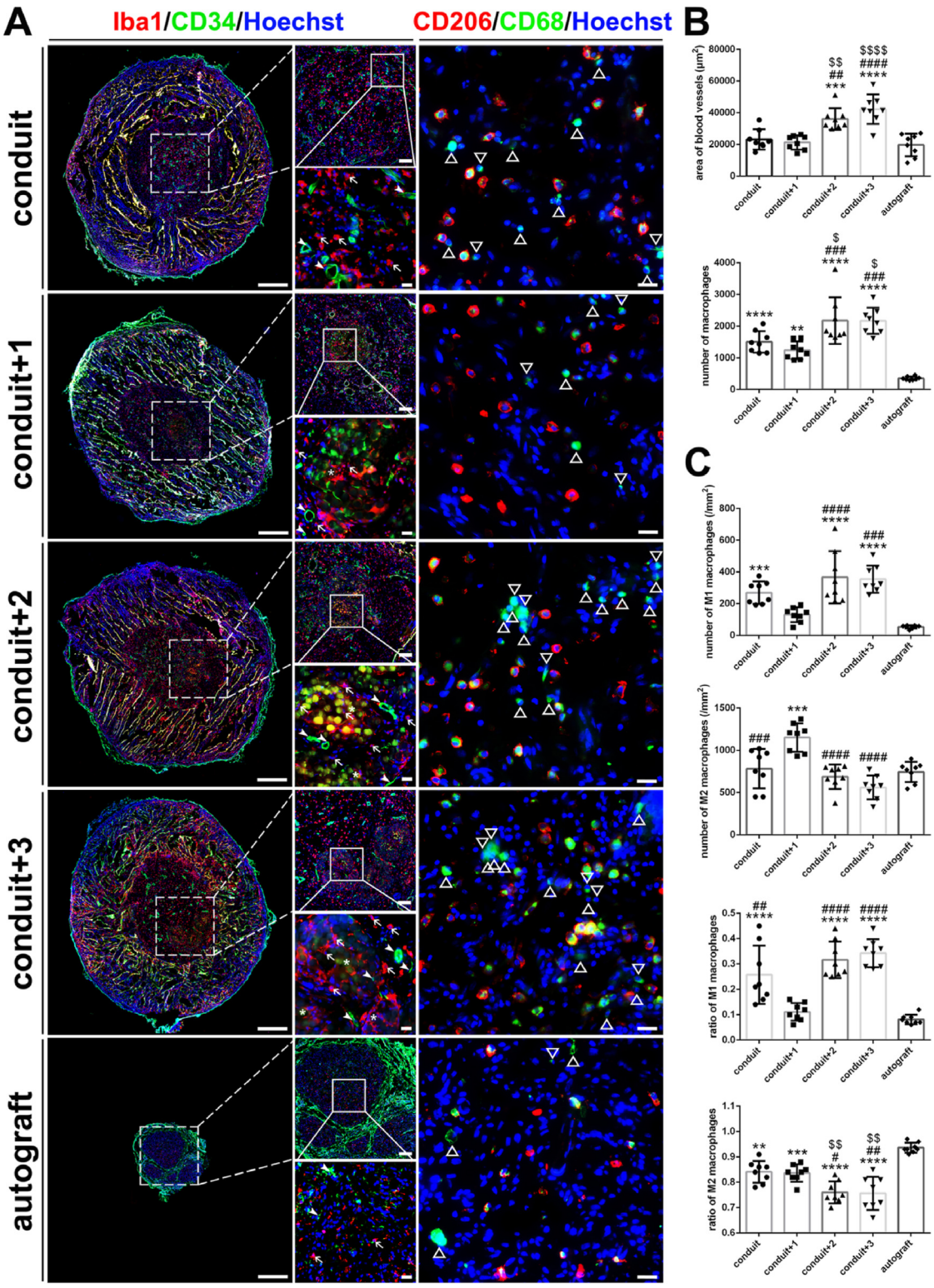

Fig. 8. The macrophage invasion and blood vessel formation of regeneration microenvironment at 4 w. The number of macrophages and blood vessels in the lumen of the nerve conduit between the conduit and conduit+1 displayed no significant difference, significantly less than the conduit+2 and conduit+3 groups. Analysis of macrophage subtypes was further performed. The M1 macrophages of conduit+1 and autograft were significantly less than those of conduit, conduit+2, and conduit+3 groups. While the M2 macrophages of conduit+1 and autograft were significantly more than those of other groups. (A) Immunohistochemical images of macrophages (Iba1+, red) and blood vessels ($CD34^+$, green) with the panoramic and local low and high magnification field of view. The arrows indicated the macrophages. The arrowheads indicated the blood vessels. The asterisks indicated the PLGA scaffolds. Scale bar, 500 μm, 100 μm, and 20 μm respectively. The M1 ($CD68^+$, green; CD206-) and M2 ($CD68^+$, green; CD206+, red) subtypes of macrophages were further illustrated. Scale bar, 20 μm. The triangles indicated the M1 macrophages. Nuclei were stained using Hoechst (blue). (B) Histograms of the areas of blood vessels and the numbers of macrophages. (C) Histograms of the numbers and ratios of M1 and M2 macrophages. *, each group vs. autograft group. #, each group vs. conduit+1 group. $, each group vs. conduit group. **, $p<0.01$; ***, $p<0.001$; ****, $p<0.0001$. #, $p<0.05$; ##, $p<0.01$; ###, $p<0.001$; ####, $p<0.0001$. $, $p<0.05$; $$, $p<0.01$; $$$$, $p<0.0001$.

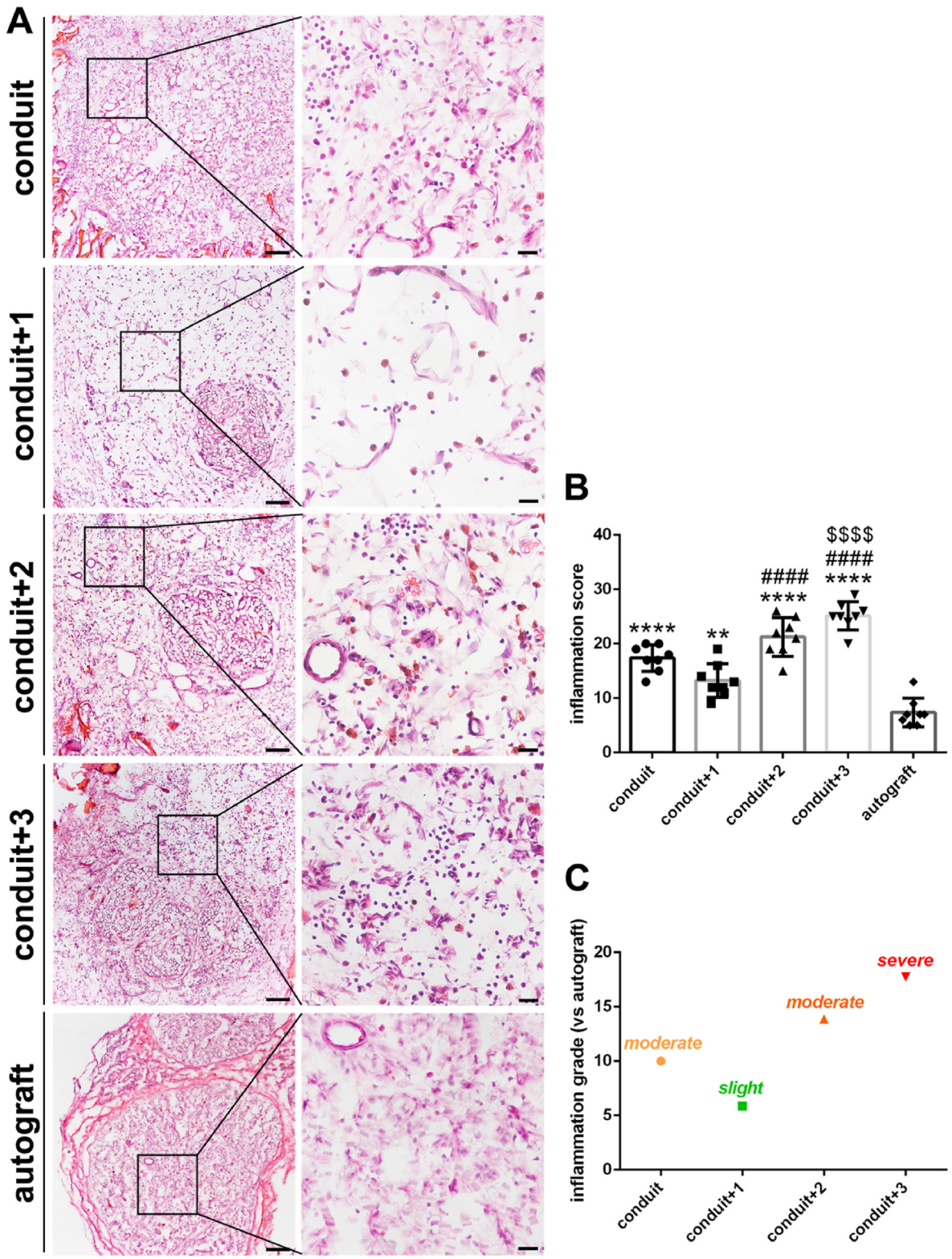

Fig. 9. The inflammation scores and grades of local regeneration microenvironment at 4 w. The autograft group demonstrated minimal local inflammation. The local inflammation of the regeneration microenvironment gradually increased from the conduit+1, conduit, conduit+2 to conduit+3 groups. The inflammation of conduit+1 was significantly lower than those of the conduit+2 and conduit+3 groups. (A) The images of HE staining of different groups. Scale bar, 100 μm, and 20 μm. (B) Histograms of the inflammation scores. *, each group vs. autograft group. #, each group vs. conduit+1 group. $, each group vs. conduit group. **, $p<0.01$; ****, $p<0.0001$. ####, $p<0.0001$. $$$$, $p<0.0001$. (C) Histograms of the inflammation grades compared with the autograft group.

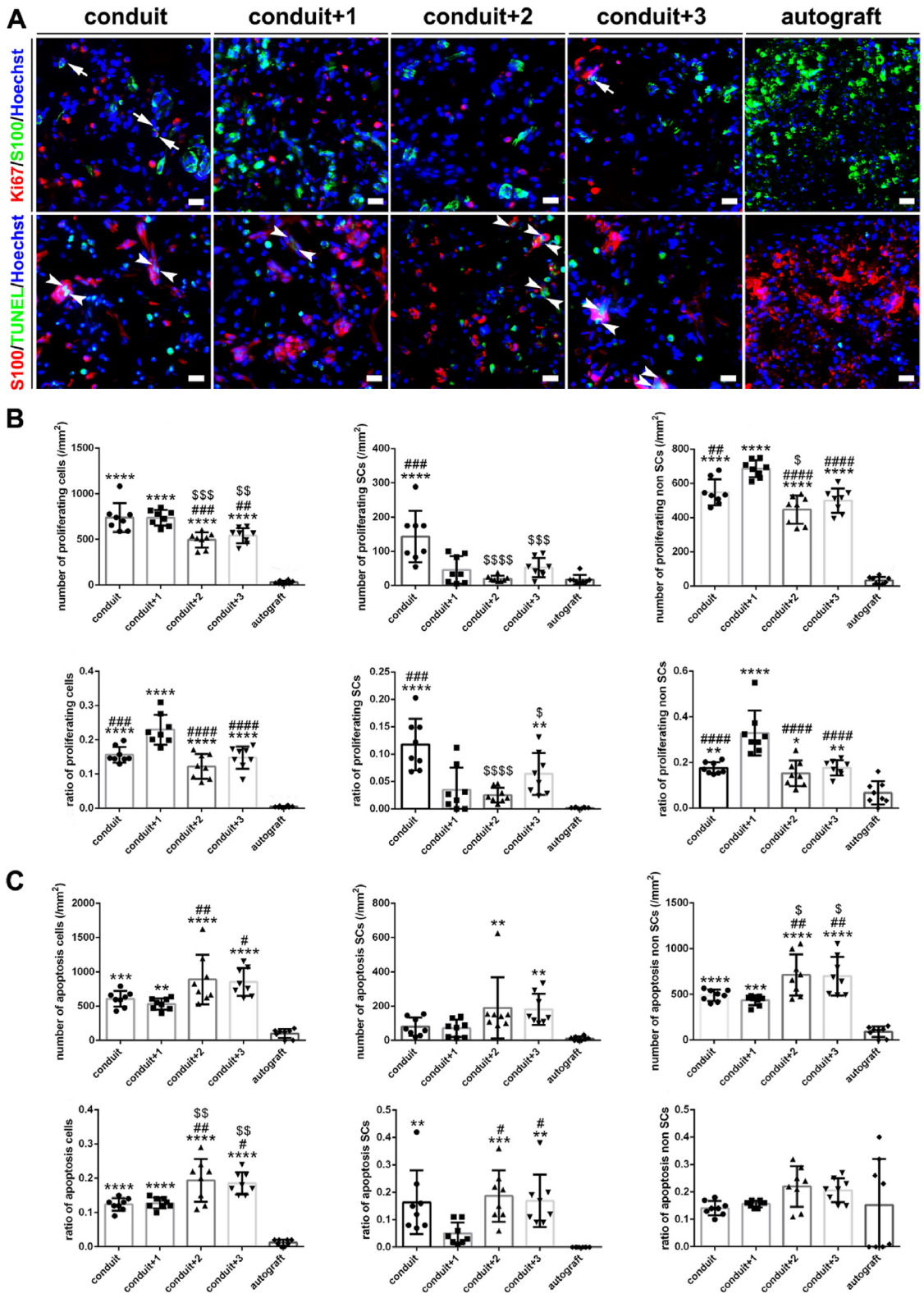

Fig. 10. The proliferation and apoptosis of cells in regeneration microenvironment at 4 w. Compared with the conduit+1, the local microenvironment of conduit, conduit+2, and conduit+3 groups more significantly inhibited cell proliferation, and the detailed investigation revealed that mainly the proliferation of non-SCs was inhibited. On the contrary, the proliferation of SCs was significantly increased of the conduit alone, which was different from the other groups. The regenerative microenvironment exerted an identical effect on cell apoptosis, including both SCs and non-SCs. The local environment of conduit+2 and conduit+3 groups induced much more cell apoptosis, indicating their conditions that seemed to be less conducive to nerve regeneration. (A) The images of cell proliferation (Ki67+, red) and apoptosis (TUNEL+, green). The SCs were marked by anti-S100 staining. Nuclei were stained using Hoechst (blue). The arrows indicated the proliferation of cells. The arrowheads indicated the apoptosis cells. Scale bar, 20 μm (B) Histograms of the numbers and ratios of proliferation cells. (C) Histograms of the numbers and ratios of apoptosis cells. *, each group vs. autograft group. #, each group vs. conduit+1 group. $, each group vs. conduit group. *, $p<0.05$; **, $p<0.01$; ***, $p<0.001$; ****, $p<0.0001$. #, $p<0.05$; ##, $p<0.01$; ###, $p<0.001$; ####, $p<0.0001$. $, $p<0.05$; $$, $p<0.01$; $$$, $p<0.001$; $$$$, $p<0.0001$.

denervation to reinnervation, that is, the process of continuous atrophy and then gradually recovering. In addition to the reinnervation of nerve regeneration to retrieve muscle functions, the treatment to prevent muscle from atrophy in the early stage of nerve injury was also of great significance and importance. Moreover, it was worth noting that the process of denervation atrophy of different target muscles was not the same exactly, which may have potential instructions for the functional recovery of the target muscles in clinic. Better muscle reinnervation of the conduit+1 was reflected in multi-dimensional evaluations. The abilities of prevention of muscle atrophy and restoration of atrophic muscle cells of conduit+1 and autograft were much stronger. The average areas of the motor endplates of conduit+1 and autograft were significantly larger than those of the other three groups at three time points.

Peripheral nerve regeneration depends on reconstruction of local regeneration microenvironment. The microenvironment contains key neural regeneration factors: immune response, intraneural vascularization, bioenergetic metabolism and bioelectrical conduction [52]. How different amounts of PLGA scaffolds affected the nerve regeneration microenvironment of TENGs was a question that we were further concerned about. It was reported that lactic acid might increase the expression of a series of pro-angiogenic factors in vascular endothelial cells and activate pro-angiogenic signaling pathways to improve angiogenesis behavior significantly [53–55]. The two groups with more PLGA scaffolds, conduit+2, and conduit+3, indeed generated more new blood vessels in the lumen of the nerve conduit. However, a significant difference in the number of blood vessels was not displayed among the conduit, conduit+1, and autograft. The results suggested that the interactions between biomaterials and body *in vivo*, and their effects of biomaterials degradation products on angiogenesis were diverse and intricate. Moreover the role of new blood vessels acting as a bridge to guide and promote migration of Schwann cells for peripheral nerve regeneration was recently reported [56,57]. However the lower number of blood vessels of conduit+1 with the better functional recovery was illustrated. Therefore, at different stages of peripheral nerve regeneration, is there a different emphasis on the role of blood vessels? Is the larger the number of blood vessels, the better the nerve regeneration? This is a small but critical issue for a deeper and comprehensive understanding of vascular factors in peripheral nerve regeneration microenvironment.

The distribution of macrophages was mainly in the lumen of conduit and secondly in the apertures of conduit wall. The macrophages in the lumen were comparatively more distributed evenly and not just concentrated around the PLGA scaffolds, which revealed that the degradation of the scaffolds mainly caused the infiltration of macrophages. The Subsequent macrophage typing detection painted a more detailed picture. The M1 macrophages were dominantly round, partly fusiform, and small, yet the M2 macrophages were spherical and large [58–60]. More meaningfully, the analysis of different types of macrophages reflected the high inflammation states of the conduit+2 and conduit+3, and revealed the slightly higher inflammation environment of the conduit compared to the conduit+1. The nerve bridge biomaterials could improve the regeneration microenvironment and promote the peripheral nerve regeneration by inducing macrophage polarization from a proinflammatory to an anti-inflammatory state [61]. Furthermore, more indicators, including other inflammatory cells, were taken into account for the inflammation assessment. The moderate inflammation of the conduit relative to the autograft was more obviously depicted in the comprehensive inflammation scoring and rating. Therefore, we believe that the slightly higher inflammation of conduit, coupled with the lack of scaffold guidance that may be more critical, together bring about its unsatisfactory effects in repairing peripheral nerve defects. A proper amount of acid degradation products of the PLGA scaffolds could neutralize the alkaline degradation products of the chitosan conduit [36], which was conducive to building a suitable microenvironment for nerve regeneration. Additionally, through the more exhaustive evaluations, conduit+2 and conduit+3 demonstrated comparatively severe inflammation of local microenvironment, which was consistent with their poor nerve regeneration results. Then as far as these two groups were concerned, the grade of inflammation of conduit+3 was slightly higher than that of conduit+2. But the difference mentioned was not incarnated in the effect of nerve regeneration, which may be due to an upper line or threshold of the adverse effects of inflammation, or other reasons. In a few of reports exploring the construction of nerve conduits for improving peripheral nerve regeneration, anti-inflammatory and anti-oxidation were often closely linked [62,63]. Whether our TENGs have the effect on scavenging local free radical oxygen requires related testing. Moreover, it is shown that the electrical conductivity in nerve regeneration microenvironment is one of the aspects worthy of attention. The nerve conduits constructed by piezoelectric materials stimulated cellular excretion of neurotrophic factors and regulated energy metabolic balance [64,65]. What is the electrical conductivity and piezoelectric properties of the chitosan conduit and PLGA scaffolds of the TENGs, and how it affects the nerve regeneration microenvironment, deserves more observation and research. In summary, our experiments dissected that the degradation of the PLGA scaffolds had a huge impact on the local regeneration microenvironment of TENGs and directly lead to the different nerve regeneration performances.

During the peripheral nerve regeneration, SCs will undergo dedifferentiation and proliferation, followed by differentiation and myelination [66–68]. In the present work, the massive proliferation of SCs should occur before the observation time point of 4 weeks after surgery. So, it showed most proliferating cells were other types, while SCs were proliferating relatively few. This may explain the number and ratio of proliferating SCs between the conduit+1, conduit+2, and conduit+3 did not show significant differences. Interestingly, the proliferation of SCs of the conduit was significantly increased compared with the other TENGs. We speculated that the abnormal increase of SC proliferation of conduit should be aroused by the lack of guiding effect of the PLGA scaffolds. The absence of PLGA scaffolds greatly delayed the differentiation and maturation of SCs that still stayed in a proliferation phase, the effect of which seemed to exceed the impact of local inflammation. Whether the acidic microenvironment imposed a direct and considerable impact on the differentiation and maturation of SCs remained to be further studied. Of course, whether the significant inhibition of the proliferation of non-SCs, such as macrophages or fibroblasts, caused by the acidification of the regenerative microenvironment exerted a visible and sizeable influence on peripheral nerve regeneration was another issue worth continuing to explore.

We provided a solid theoretical basis for the quantity control of the PLGA scaffolds into the chitosan neural conduit, and have an intuitive and clear understanding of characteristics of PLGA and their applications in nerve regeneration. Under the optimal dosage condition, the positive and negative effects of the biomaterial could reach a delicate balance. The safety and effectiveness of tissue engineered products are critical to their clinical applications. The results supplied the experimental support for approval and marketing of our first-generation patented peripheral nerve tissue engineered product that had completed the clinical trials in China. The new issues discovered expanded the vision for further improvement of our product and design and development of a new generation of TENGs. In addition, it expands more directions and enlightenments for studying and applying polyester materials in other tissue regeneration fields. Our experiment also has its limitations in the depth of exploration. Behind a series of phenomena presented, our investigation did not involve analyzing of molecular mechanism regulations, which is crucial to reveal the essence of the problem. Apart from this, our understanding of the use of PLGA, or other similar biological materials, is in its infancy in regenerative medicine, and numerous fundamental questions remain. According to the specific conditions of regenerated tissues and organs, the appropriate amount of polymer materials or the complementary combination of other biomaterials may be the answers.

Author statement

Panjian Lu: Formal analysis, Investigation, Visualization; Gang Wang: Validation, Visualization; Tianmei Qian: Investigation; Xiaodong Cai: Resources; Ping Zhang: Investigation; Meiyuan Li: Validation; Yinying Shen: Investigation; Chengbin Xue: Writing – original draft, Writing – review & editing, Supervision; Hongkui Wang: Conceptualization, Methodology, Writing – original draft, Writing – review & editing, Visualization, Supervision.

Funding

This work was supported by grants from the National Natural Science Foundation of China (Grant No. 31730031, 81,901,256, 81873767, 82172104), National Key Research and Development Program of China (Grant No. 2017YFA0104703), Jiangsu Provincial Key Medical Center and Priority Academic Program Development of Jiangsu Higher Education Institutions (PAPD).

Declarations

Availability of data and materials

All data generated or analyzed during this study are included in this published article and its supplementary information files.

Competing interests

The authors declare that they have no competing interests.

Authors' contributions

H.W. and P.L. designed the experiments; H.W. and P.L. analyzed data; P.L., G.W., T.Q., X.C., P.Z., M.L., Y.S. and C.X. performed the experiments; H.W. and C.X. wrote and revised the manuscript. All authors have read and approved the final manuscript.

Declaration of competing interest

The authors declare that they have no known competing financial interests or personal relationships that could have appeared to influence the work reported in this paper.

Appendix A. Supplementary data

Supplementary data to this article can be found online at https://doi.org/10.1016/j.mtbio.2021.100158.

References

[1] W.H. Chooi, S.Y. Chew, Modulation of cell-cell interactions for neural tissue engineering: potential therapeutic applications of cell adhesion molecules in nerve regeneration, Biomaterials 197 (2019) 327–344.
[2] M. Jahromi, S. Razavi, A. Bakhtiari, The advances in nerve tissue engineering: from fabrication of nerve conduit to in vivo nerve regeneration assays, Journal of tissue engineering and regenerative medicine 13 (11) (2019) 2077–2100.
[3] E. Onode, T. Uemura, K. Takamatsu, T. Yokoi, K. Shintani, S. Hama, Y. Miyashima, M. Okada, H. Nakamura, Bioabsorbable nerve conduits three-dimensionally coated with human induced pluripotent stem cell-derived neural stem/progenitor cells promote peripheral nerve regeneration in rats, Sci. Rep. 11 (1) (2021) 4204.
[4] Y. Yang, F. Ding, J. Wu, W. Hu, W. Liu, J. Liu, X. Gu, Development and evaluation of silk fibroin-based nerve grafts used for peripheral nerve regeneration, Biomaterials 28 (36) (2007) 5526–5535.
[5] K.S. Katiyar, L.A. Struzyna, J.P. Morand, J.C. Burrell, B. Clements, F.A. Laimo, K.D. Browne, J. Kohn, Z. Ali, H.C. Ledebur, D.H. Smith, D.K. Cullen, Tissue engineered axon tracts serve as living scaffolds to accelerate axonal regeneration and functional recovery following peripheral nerve injury in rats, Front Bioeng Biotechnol 8 (2020) 492.
[6] Z. Bin, Z. Zhihu, M. Jianxiong, M. Xinlong, Repairing peripheral nerve defects with revascularized tissue-engineered nerve based on a vascular endothelial growth factor-heparin sustained release system, Journal of tissue engineering and regenerative medicine 14 (6) (2020) 819–828.
[7] J.Y. Lee, Y.H. Kim, B.Y. Kim, D.H. Jang, S.W. Choi, S.H. Joen, H. Kim, S.U. Lee, Peripheral Nerve Regeneration Using a Nerve Conduit with Olfactory Ensheathing Cells in a Rat Model, Tissue Engineering and Regenerative Medicine, 2021.
[8] W. Huang, R. Begum, T. Barber, V. Ibba, N.C. Tee, M. Hussain, M. Arastoo, Q. Yang, L.G. Robson, S. Lesage, T. Gheysens, N.J. Skaer, D.P. Knight, J.V. Priestley, Regenerative potential of silk conduits in repair of peripheral nerve injury in adult rats, Biomaterials 33 (1) (2012) 59–71.
[9] A. Zaszczynska, P. Sajkiewicz, A. Gradys, Piezoelectric scaffolds as smart materials for neural tissue engineering, Polymers 12 (1) (2020).
[10] S.G. Kim, Immunomodulation and smart materials for maxillofacial tissue engineering, Maxillofac Plast Reconstr Surg 42 (1) (2020) 3.
[11] N. Ghane, S. Khalili, S. Nouri Khorasani, R. Esmaeely Neisiany, O. Das, S. Ramakrishna, Regeneration of the peripheral nerve via multifunctional electrospun scaffolds, J. Biomed. Mater. Res. 109 (4) (2021) 437–452.
[12] S.H. Chang, Y.Y. Lin, G.J. Wu, C.H. Huang, G.J. Tsai, Effect of chitosan molecular weight on anti-inflammatory activity in the RAW 264.7 macrophage model, Int. J. Biol. Macromol. 131 (2019) 167–175.
[13] M.M. Islam, M. Shahruzzaman, S. Biswas, M. Nurus Sakib, T.U. Rashid, Chitosan based bioactive materials in tissue engineering applications-A review, Bioact Mater 5 (1) (2020) 164–183.
[14] S. Abdulghani, G.R. Mitchell, Biomaterials for in situ tissue regeneration: a review, Biomolecules 9 (11) (2019).
[15] A.K. Gaharwar, I. Singh, A. Khademhosseini, Engineered biomaterials for in situ tissue regeneration: a Review, Nat. Rev. Mater. 5 (9) (2020) 686–705.
[16] R.D. Alvites, M.V. Branquinho, A.C. Sousa, I. Amorim, R. Magalhaes, F. Joao, D. Almeida, S. Amado, J. Prada, I. Pires, F. Zen, S. Raimondo, A.L. Luis, S. Geuna, A.S.P. Varejao, A.C. Mauricio, Combined use of chitosan and olfactory mucosa mesenchymal stem/stromal cells to promote peripheral nerve regeneration in vivo, Stem Cell. Int. 2021 (2021) 6613029.
[17] X. Tang, C. Xue, Y. Wang, F. Ding, Y. Yang, X. Gu, Bridging peripheral nerve defects with a tissue engineered nerve graft composed of an in vitro cultured nerve equivalent and a silk fibroin-based scaffold, Biomaterials 33 (15) (2012) 3860–3867.
[18] D.F. Williams, Essential Biomaterials Science.
[19] K. Xi, Y. Gu, J. Tang, H. Chen, Y. Xu, L. Wu, F. Cai, L. Deng, H. Yang, Q. Shi, W. Cui, L. Chen, Microenvironment-responsive immunoregulatory electrospun fibers for promoting nerve function recovery, Nat. Commun. 11 (1) (2020) 4504.
[20] V. Bucan, D. Vaslaitis, C.T. Peck, S. Strauss, P.M. Vogt, C. Radtke, Effect of exosomes from rat adipose-derived mesenchymal stem cells on neurite outgrowth and sciatic nerve regeneration after crush injury, Mol. Neurobiol. 56 (3) (2019) 1812–1824.
[21] M.P. Clements, E. Byrne, L.F. Camarillo Guerrero, A.L. Cattin, L. Zakka, A. Ashraf, J.J. Burden, S. Khadayate, A.C. Lloyd, S. Marguerat, S. Parrinello, The wound microenvironment reprograms Schwann cells to invasive mesenchymal-like cells to drive peripheral nerve regeneration, Neuron 96 (1) (2017) 98–114 e7.
[22] X. Wang, W. Hu, Y. Cao, J. Yao, J. Wu, X. Gu, Dog sciatic nerve regeneration across a 30-mm defect bridged by a chitosan/PGA artificial nerve graft, Brain : J. Neurol. 128 (Pt 8) (2005) 1897–1910.
[23] Y. Gu, J. Zhu, C. Xue, Z. Li, F. Ding, Y. Yang, X. Gu, Chitosan/silk fibroin-based, Schwann cell-derived extracellular matrix-modified scaffolds for bridging rat sciatic nerve gaps, Biomaterials 35 (7) (2014) 2253–2263.
[24] X. Gu, F. Ding, Y. Yang, J. Liu, Construction of tissue engineered nerve grafts and their application in peripheral nerve regeneration, Prog. Neurobiol. 93 (2) (2011) 204–230.
[25] N. Hu, H. Wu, C. Xue, Y. Gong, J. Wu, Z. Xiao, Y. Yang, F. Ding, X. Gu, Long-term outcome of the repair of 50 mm long median nerve defects in rhesus monkeys with marrow mesenchymal stem cells-containing, chitosan-based tissue engineered nerve grafts, Biomaterials 34 (1) (2013) 100–111.
[26] Y. Yuan, P. Zhang, Y. Yang, X. Wang, X. Gu, The interaction of Schwann cells with chitosan membranes and fibers in vitro, Biomaterials 25 (18) (2004) 4273–4278.
[27] D. Liu, D. Mi, T. Zhang, Y. Zhang, J. Yan, Y. Wang, X. Tan, Y. Yuan, Y. Yang, X. Gu, W. Hu, Tubulation repair mitigates misdirection of regenerating motor axons across a sciatic nerve gap in rats, Sci. Rep. 8 (1) (2018) 3443.
[28] Y. Wang, Y. Zhao, C. Sun, W. Hu, J. Zhao, G. Li, L. Zhang, M. Liu, Y. Liu, F. Ding, Y. Yang, X. Gu, Chitosan degradation products promote nerve regeneration by stimulating Schwann cell proliferation via miR-27a/FOXO1 Axis, Mol. Neurobiol. 53 (1) (2016) 28–39.
[29] Y. Zhao, Y. Wang, J. Gong, L. Yang, C. Niu, X. Ni, Y. Wang, S. Peng, X. Gu, C. Sun, Y. Yang, Chitosan degradation products facilitate peripheral nerve regeneration by improving macrophage-constructed microenvironments, Biomaterials 134 (2017) 64–77.
[30] Y.X. Wu, H. Ma, J.L. Wang, W. Qu, Production of chitosan scaffolds by lyophilization or electrospinning: which is better for peripheral nerve regeneration? Neural regeneration research 16 (6) (2021) 1093–1098.
[31] W. Hu, J. Gu, A. Deng, X. Gu, Polyglycolic acid filaments guide Schwann cell migration in vitro and in vivo, Biotechnol. Lett. 30 (11) (2008) 1937–1942.
[32] J. Sun, W. He, A. Meng, [Study on cyto-compatibility of PGLA film for periodontal guided tissue regeneration], Sheng Wu yi xue gong cheng xue za zhi, Journal of biomedical engineering = Shengwu yixue gongchengxue zazhi 20 (3) (2003) 388–391.
[33] Y. Peng, K.Y. Li, Y.F. Chen, X.J. Li, S. Zhu, Z.Y. Zhang, X. Wang, L.N. Duan, Z.J. Luo, J.J. Du, J.C. Wang, Beagle sciatic nerve regeneration across a 30mm defect bridged by chitosan/PGA artificial nerve grafts, Injury 49 (8) (2018) 1477–1484.

[34] E.J. Kim, S.J. Yoon, G.D. Yeo, C.M. Pai, I.K. Kang, Preparation of biodegradable PLA/PLGA membranes with PGA mesh and their application for periodontal guided tissue regeneration, Biomed. Mater. 4 (5) (2009), 055001.
[35] W. Zeng, H. Hui, Z. Liu, Z. Chang, M. Wang, B. He, D. Hao, TPP ionically cross-linked chitosan/PLGA microspheres for the delivery of NGF for peripheral nerve system repair, Carbohydr. Polym. 258 (2021) 117684.
[36] Y. Shen, T. Tu, B. Yi, X. Wang, H. Tang, W. Liu, Y. Zhang, Electrospun acid-neutralizing fibers for the amelioration of inflammatory response, Acta Biomater. 97 (2019) 200–215.
[37] T. Fabre, M. Schappacher, R. Bareille, B. Dupuy, A. Soum, J. Bertrand-Barat, C. Baquey, Study of a (trimethylenecarbonate-co-epsilon-caprolactone) polymer–part 2: in vitro cytocompatibility analysis and in vivo ED1 cell response of a new nerve guide, Biomaterials 22 (22) (2001) 2951–2958.
[38] J. Hazan, A.J. Azzi, S. Thibaudeau, Surgical fixation of metacarpal shaft fractures using absorbable implants: a systematic review of the literature, Hand 14 (1) (2019) 19–26.
[39] U. Paivarinta, O. Bostman, A. Majola, T. Toivonen, P. Tormala, P. Rokkanen, Intraosseous cellular response to biodegradable fracture fixation screws made of polyglycolide or polylactide, Arch. Orthop. Trauma Surg. 112 (2) (1993) 71–74.
[40] P.J. Lu, G. Wang, X.D. Cai, P. Zhang, H.K. Wang, Sequencing analysis of matrix metalloproteinase 7-induced genetic changes in Schwann cells, Neural regeneration research 15 (11) (2020) 2116–2122.
[41] H. Wang, P. Zhang, J. Yu, F. Zhang, W. Dai, S. Yi, Matrix metalloproteinase 7 promoted Schwann cell migration and myelination after rat sciatic nerve injury, Mol. Brain 12 (1) (2019) 101.
[42] H. Wang, Q. Zhao, W. Zhao, Q. Liu, X. Gu, Y. Yang, Repairing rat sciatic nerve injury by a nerve-growth-factor-loaded, chitosan-based nerve conduit, Biotechnol. Appl. Biochem. 59 (5) (2012) 388–394.
[43] Y. Ikarashi, K. Toyoda, N. Ohsawa, T. Uchima, T. Tsuchiya, M. Kaniwa, M. Sato, M. Takahashi, A. Nakamura, Comparative studies by cell culture and in vivo implantation test on the toxicity of natural rubber latex materials, J. Biomed. Mater. Res. 26 (3) (1992) 339–356.
[44] A. Pizzoferrato, G. Ciapetti, L. Savarino, S. Stea, C. Tarabusi, Results of histological grading on 100 cases of hip prosthesis failure, Biomaterials 9 (4) (1988) 314–318.
[45] Y. Haishima, K. Isama, C. Hasegawa, T. Yuba, A. Matsuoka, A development and biological safety evaluation of novel PVC medical devices with surface structures modified by UV irradiation to suppress plasticizer migration, J. Biomed. Mater. Res. 101 (9) (2013) 2630–2643.
[46] T.T. Ngo, P.J. Waggoner, A.A. Romero, K.D. Nelson, R.C. Eberhart, G.M. Smith, Poly(L-Lactide) microfilaments enhance peripheral nerve regeneration across extended nerve lesions, J. Neurosci. Res. 72 (2) (2003) 227–238.
[47] K. Kohno, S. Koya-Miyata, A. Harashima, T. Tsukuda, M. Katakami, T. Ariyasu, S. Ushio, K. Iwaki, Inflammatory M1-like macrophages polarized by NK-4 undergo enhanced phenotypic switching to an anti-inflammatory M2-like phenotype upon co-culture with apoptotic cells, J. Inflamm. 18 (1) (2021) 2.
[48] M.D. Sarker, S. Naghieh, A.D. McInnes, D.J. Schreyer, X. Chen, Regeneration of peripheral nerves by nerve guidance conduits: influence of design, biopolymers, cells, growth factors, and physical stimuli, Prog. Neurobiol. 171 (2018) 125–150.
[49] W. Zhao, J. Li, K. Jin, W. Liu, X. Qiu, C. Li, Fabrication of functional PLGA-based electrospun scaffolds and their applications in biomedical engineering, Materials science & engineering, C, Materials for biological applications 59 (2016) 1181–1194.
[50] T.B. Bini, S. Gao, X. Xu, S. Wang, S. Ramakrishna, K.W. Leong, Peripheral nerve regeneration by microbraided poly(L-lactide-co-glycolide) biodegradable polymer fibers, J. Biomed. Mater. Res. 68 (2) (2004) 286–295.
[51] M.C. Lu, Y.T. Huang, J.H. Lin, C.H. Yao, C.W. Lou, C.C. Tsai, Y.S. Chen, Evaluation of a multi-layer microbraided polylactic acid fiber-reinforced conduit for peripheral nerve regeneration, J. Mater. Sci. Mater. Med. 20 (5) (2009) 1175–1180.
[52] Y. Qian, H. Lin, Z. Yan, J. Shi, C. Fan, Functional nanomaterials in peripheral nerve regeneration: scaffold design, chemical principles and microenvironmental remodeling, Mater. Today (2021), https://doi.org/10.1016/j.mattod.2021.09.014.
[53] F. Vegran, R. Boidot, C. Michiels, P. Sonveaux, O. Feron, Lactate influx through the endothelial cell monocarboxylate transporter MCT1 supports an NF-kappaB/IL-8 pathway that drives tumor angiogenesis, Cancer Res. 71 (7) (2011) 2550–2560.
[54] G.X. Ruan, A. Kazlauskas, Lactate engages receptor tyrosine kinases Axl, Tie2, and vascular endothelial growth factor receptor 2 to activate phosphoinositide 3-kinase/Akt and promote angiogenesis, J. Biol. Chem. 288 (29) (2013) 21161–21172.
[55] X.F. Hu, Y.F. Feng, G. Xiang, W. Lei, L. Wang, Lactic acid of PLGA coating promotes angiogenesis on the interface between porous titanium and diabetic bone, J. Mater. Chem. B 6 (15) (2018) 2274–2288.
[56] P. Muangsanit, V. Roberton, E. Costa, J.B. Phillips, Engineered aligned endothelial cell structures in tethered collagen hydrogels promote peripheral nerve regeneration, Acta Biomater. 126 (2021) 224–237.
[57] A.L. Cattin, J.J. Burden, L. Van Emmenis, F.E. Mackenzie, J.J. Hoving, N. Garcia Calavia, Y. Guo, M. McLaughlin, L.H. Rosenberg, V. Quereda, D. Jamecna, I. Napoli, S. Parrinello, T. Enver, C. Ruhrberg, A.C. Lloyd, Macrophage-induced blood vessels guide Schwann cell-mediated regeneration of peripheral nerves, Cell 162 (5) (2015) 1127–1139.
[58] C.W.t. Shields, M.A. Evans, L.L. Wang, N. Baugh, S. Iyer, D. Wu, Z. Zhao, A. Pusuluri, A. Ukidve, D.C. Pan, S. Mitragotri, Cellular backpacks for macrophage immunotherapy, Sci Adv 6 (18) (2020) eaaz6579.
[59] E. Ydens, L. Amann, B. Asselbergh, C.L. Scott, L. Martens, D. Sichien, O. Mossad, T. Blank, S. De Prijck, D. Low, T. Masuda, Y. Saeys, V. Timmerman, R. Stumm, F. Ginhoux, M. Prinz, S. Janssens, M. Guilliams, Profiling peripheral nerve macrophages reveals two macrophage subsets with distinct localization, transcriptome and response to injury, Nat. Neurosci. 23 (5) (2020) 676–689.
[60] P.L. Graney, S. Ben-Shaul, S. Landau, A. Bajpai, B. Singh, J. Eager, A. Cohen, S. Levenberg, K.L. Spiller, Macrophages of diverse phenotypes drive vascularization of engineered tissues, Sci Adv 6 (18) (2020), eaay6391.
[61] Y. Qian, Y. Cheng, Y.M. Ouyang, W.E. Yuan, C.Y. Fan, Multilayered spraying and gradient dotting of nanodiamond-polycaprolactone guidance channels for restoration of immune homeostasis, NPG Asia Mater. 11 (2019).
[62] Y. Qian, Z.X. Yao, X. Wang, Y. Cheng, Z.W. Fang, W.E. Yuan, C.Y. Fan, Y.M. Ouyang, (-)-Epigallocatechin gallate-loaded polycaprolactone scaffolds fabricated using a 3D integrated moulding method alleviate immune stress and induce neurogenesis, Cell Prolif 53 (1) (2020).
[63] Y. Qian, Q.X. Han, X.T. Zhao, H. Li, W.E. Yuan, C.Y. Fan, Asymmetrical 3D nanoceria channel for severe neurological defect regeneration, Iscience 12 (2019) 216(. -+).
[64] Y. Qian, Y. Xu, Z.W. Yan, Y. Jin, X. Chen, W.E. Yuan, C.Y. Fan, Boron nitride nanosheets functionalized channel scaffold favors microenvironment rebalance cocktail therapy for piezocatalytic neuronal repair, Nanomater. Energy 83 (2021).
[65] Y. Qian, Y. Cheng, J.L. Song, Y. Xu, W.E. Yuan, C.Y. Fan, X.Y. Zheng, Mechano-informed biomimetic polymer scaffolds by incorporating self-powered zinc oxide nanogenerators enhance motor recovery and neural function, Small 16 (32) (2020).
[66] S.N. Rao, D.D. Pearse, Regulating axonal responses to injury: the intersection between signaling pathways involved in axon myelination and the inhibition of axon regeneration, Front. Mol. Neurosci. 9 (2016) 33.
[67] K.R. Jessen, R. Mirsky, A.C. Lloyd, Schwann cells: development and role in nerve repair, Cold Spring Harb Perspect Biol 7 (7) (2015), a020487.
[68] K.R. Jessen, R. Mirsky, The repair Schwann cell and its function in regenerating nerves, J. Physiol. 594 (13) (2016) 3521–3531.